



HAL
open science

Modeling the effects of morphological anisotropy in transformation plasticity of metals and alloys

Youssri El Majaty, Le-Hung Tran, Jean-Baptiste Leblond, Renald Brenner

► **To cite this version:**

Youssri El Majaty, Le-Hung Tran, Jean-Baptiste Leblond, Renald Brenner. Modeling the effects of morphological anisotropy in transformation plasticity of metals and alloys. *International Journal of Solids and Structures*, 2023, 282, pp.112447. 10.1016/j.ijsolstr.2023.112447 . hal-04189075

HAL Id: hal-04189075

<https://hal.science/hal-04189075>

Submitted on 28 Aug 2023

HAL is a multi-disciplinary open access archive for the deposit and dissemination of scientific research documents, whether they are published or not. The documents may come from teaching and research institutions in France or abroad, or from public or private research centers.

L'archive ouverte pluridisciplinaire **HAL**, est destinée au dépôt et à la diffusion de documents scientifiques de niveau recherche, publiés ou non, émanant des établissements d'enseignement et de recherche français ou étrangers, des laboratoires publics ou privés.

Modeling the effects of morphological anisotropy in transformation plasticity of metals and alloys

Youssri El Majaty, Le-Hung Tran, Jean-Baptiste Leblond*,
Renald Brenner

*Sorbonne Université, CNRS, UMR 7190, Institut Jean Le Rond d'Alembert, F-75005 Paris,
France*

Abstract

There has recently been renewed interest in the theoretical modeling of Greenwood and Johnson (1965)'s mechanism of transformation plasticity of metals and alloys. Neglecting the effects of elasticity and using an analogy with problems of ductile rupture, El Majaty *et al.* (2018) transposed to transformation plasticity the powerful methods of limit-analysis usually applied to plastic porous materials, by replacing empty voids through nuclei of daughter-phase expanding within a shrinking matrix of mother-phase. This work, based on the hypothesis of spherical growth of nuclei of daughter-phase implying overall geometric isotropy, disregarded the frequently observed effects of *morphological anisotropies*. The present study introduces these effects by extending El Majaty *et al.* (2018)'s limit-analysis-based approach to *spheroidal*, instead of *spherical*, nuclei of daughter-phase. A typical consequence of the morphological anisotropy thus introduced is the prediction of a *nonzero transformation plastic strain even in the absence of any external stress applied*. The theory is completed by FFT-based numerical simulations. While essentially confirming the theory, these simulations suggest to overhaul it through heuristic corrections of the expression of the transformation plastic strain rate, accounting for the presence and influence of elasticity.

Keywords : Transformation plasticity; Greenwood-Johnson's mechanism; morphological anisotropies; limit-analysis; FFT micromechanical simulations

1 Introduction

The anomalous plastic behavior (temporary increase of deformability) of metals and alloys during phase transformations, especially during the cooling period of thermomechanical treatments, is classically termed *transformation plasticity*. It is commonly attributed to two mechanisms: (i) plastic *accommodation*, within the weaker mother-phase, of the internal stresses due to the difference of specific volume between the phases - the volumetric part of the transformation strain (Greenwood and Johnson, 1965); (ii)

* Corresponding author.

external-stress-induced *orientation*, within the daughter-phase, of the deviatoric part of the transformation strain (Magee, 1966). Among the large body of literature devoted to the subject, a non-exhaustive list of significant experimental, theoretical and numerical works includes, in addition to the seminal papers of Greenwood and Johnson (1965) and Magee (1966), those of Leblond *et al.* (1986a,b, 1989); Ganghoffer *et al.* (1993); Diani *et al.* (1995); Cherkaoui *et al.* (2000); Coret *et al.* (2002); Taleb and Sidoroff (2003); Vincent *et al.* (2003); Coret *et al.* (2004); Barbe *et al.* (2007, 2008); Barbe and Quey (2011); Fischlschweiger *et al.* (2012); Weisz-Paltrault (2017). Within this list, works devoted to modeling generally focussed on Greenwood and Johnson (1965)'s mechanism, more amenable by its purely mechanical nature to some theoretical treatment, than that of Magee (1966) involving complex metallurgical aspects. Such a restriction is sufficient in many practical cases, as discussed in Appendix B of (El Majaty *et al.*, 2018).

A new avenue to the theoretical study and modeling of Greenwood and Johnson (1965)'s mechanism - again disregarding that of Magee (1966), in line with most previous theoretical works - was recently opened by El Majaty *et al.* (2018). First, these authors remarked that neglecting the effects of elasticity, following the classical work of Leblond *et al.* (1989) and many subsequent ones, permitted to employ limit-analysis, *the* powerful theory for rigid-plastic materials developed in the 50's by Hill (1951) and Drucker *et al.* (1952). (For a recent, brief but comprehensive summary of the theory, see Leblond *et al.* (2018)). Second, they noted an analogy between *ductile rupture*, involving materials containing empty, stress-free voids, and *transformation plasticity*, involving some mother-phase containing growing nuclei of daughter-phase; the sole difference being, in the second situation, the presence within the matrix of some internal loading arising from the volumetric part of the transformation strain (Greenwood and Johnson (1965)'s mechanism). On such bases, they extended Monchiet *et al.* (2011)'s limit-analysis-based study of a hollow plastic sphere containing a spherical concentric stress-free void, so as to include an additional internal loading on the void's boundary. This led to the definition of a refined model of Greenwood and Johnson (1965)'s mechanism of transformation plasticity, essentially confirming the much earlier and cruder model of Leblond *et al.* (1989), but improving it through incorporation of new effects such as the nonlinear increase of the transformation plastic strain with the stress applied - well-documented experimentally but hitherto ignored by micromechanical analyses.

El Majaty *et al.* (2018)'s analysis and model were completed by El Majaty *et al.* (2021), using an efficient FFT-based numerical homogenization method (Moulinec and Suquet, 1998), by simulations of large RVEs containing numerous nuclei of daughter-phase gradually growing within some shrinking mother-phase. In these computations, phase transformation at a given discretization point was simulated by switching the local values of the yield stress and specific volume from these of the mother-phase to those of the daughter-phase; thus giving rise in a natural way to Greenwood and Johnson (1965)'s mechanism, as a consequence of the microplasticity resulting from incompatibilities of specific volume between the coexisting phases. The numerical values of the transformation plastic strain were found to agree very well with both the theoretical predictions of El Majaty *et al.* (2018)'s new theory and Desalos (1981)'s old, but high quality experimental measurements for the A 508 Cl. 3 steel.

These works however relied - like previous ones - on the hypothesis of *spherical* shape of the growing nuclei of daughter-phase, implying isotropy of the macrostructure. Such a hypothesis bears important consequences. For instance, in the absence of any external stress applied, the transformation plastic strain is inevitably predicted to be zero, as a byproduct of macroscopic isotropy of the geometric and mechanical state combined with plastic incompressibility of the deforming matrix (Leblond *et al.*, 1986a). Such a prediction is frequently fulfilled. But it is also often in contradiction with experimental studies, an example being Desalos (1981)'s seminal work on transformation plasticity in laminated plates containing long inclusions, generating similarly elongated nuclei of daughter-phase during the transformation: Fig. 1 shows that in the absence of any stress applied, the strain observed depended on the direction of measurement (parallel to the main dimension of the specimen), relative to the orientation of the elongated nuclei of daughter-phase (parallel to the rolling direction) - thus clearly evidencing a nonzero, anisotropic transformation plastic strain. In view of the major impact of transformation plasticity upon residual stresses and distortions resulting from thermomechanical processes (see the works of Miyao *et al.* (1986); Fukumoto *et al.* (2001); Taleb *et al.* (2004), among many others), such an effect is bound to have a significant influence upon these features of major practical interest. Its modeling represents an important, non-trivial challenge.

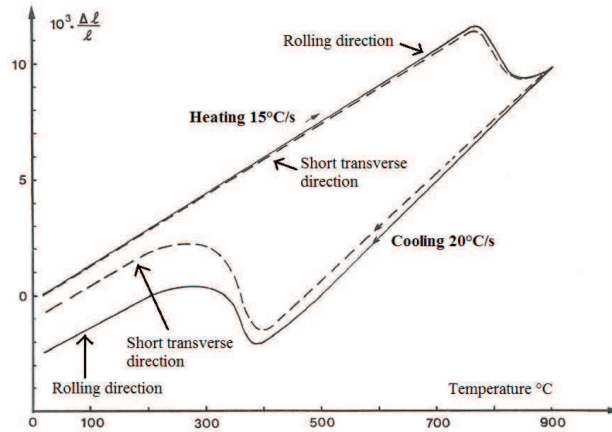


Fig. 1. Free dilatometry curves obtained by Desalos (1981) on specimens extracted in various directions from laminated plates of A 508 Cl. 3 steel. (Reprinted with permission).

The aim of this paper is precisely to overcome the restriction of previous theoretical analyses to nuclei of daughter-phase of *spherical* shape, by considering nuclei of a more general, *prolate spheroidal* shape, schematizing those encountered in laminated plates. Like in our previous work (El Majaty *et al.*, 2018) - and again disregarding Magee (1966)'s mechanism - we shall use the analogy between ductile rupture and transformation plasticity explained above; but now employing as a basis, instead of Monchiet *et al.* (2011)'s work on ductile rupture with spherical voids, their more recent work involving spheroidal ones (Monchiet *et al.*, 2014). Our ultimate goal is to pave the way to more accurate predictions of residual stresses and distortions due to thermomechanical processes, through possible use in FE codes of a more refined model of transformation plasticity including morphological anisotropy effects.

The paper is organized as follows:

- Section 2 extends Monchiet *et al.* (2014)'s study, based on the powerful kinematic approach of limit-analysis, of a plastic porous RVE containing a stress-free spheroidal void, by adding a possible internal loading applied on the void's boundary.
- Section 3 applies the results obtained to the modeling of Greenwood and Johnson (1965)'s mechanism of transformation plasticity involving elongated growing nuclei of daughter-phase. Particular, though not exclusive attention is paid to the special case of a zero external stress applied.
- Finally Section 4 presents results of some FFT-based numerical simulations of large RVEs, analogous to those of El Majaty *et al.* (2021) but for the spheroidal, instead of spherical shape of the growing nuclei of daughter-phase. Special attention is paid to the influence of elasticity disregarded by the theoretical model based on limit-analysis.

2 Limit-analysis of a hollow prolate spheroidal cell subjected to external and internal loadings

2.1 The prolate spheroidal geometry

We first introduce some basic notions and notations pertaining to the prolate spheroidal geometry. We thus consider (Fig. 2) a prolate spheroid of center O and axis of rotational symmetry Ox_3 ; additional perpendicular axes Ox_1, Ox_2 are chosen arbitrarily within the plane orthogonal to Ox_3 so as to define a Cartesian frame (O, x_1, x_2, x_3) , with associated orthonormal basis $(\mathbf{e}_1, \mathbf{e}_2, \mathbf{e}_3)$. The semi-length of the major axis of the spheroid, parallel to the direction x_3 , is denoted a_1 , and the common semi-length of the perpendicular minor axes is denoted b_1 ($a_1 > b_1$).

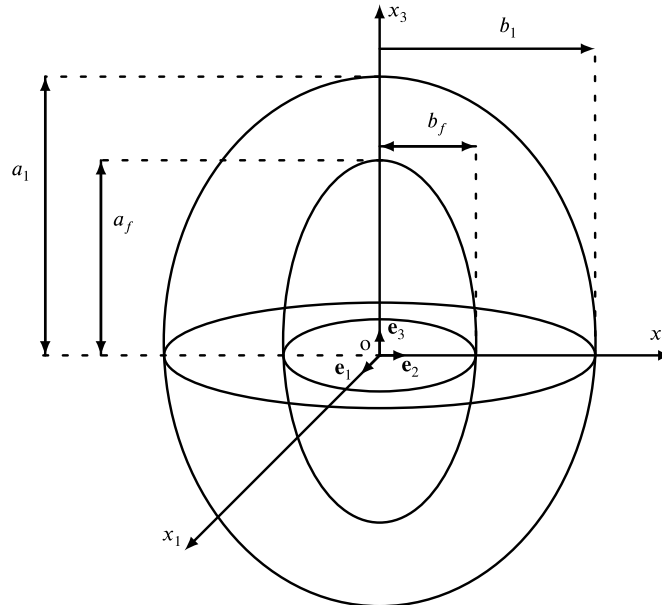


Fig. 2. The prolate spheroidal geometry: basic notations.

Within this spheroid, we consider the family of internal prolate *confocal* spheroids, indexed

by the ratio $f = \frac{\text{volume of internal spheroid}}{\text{volume of external spheroid}}$ - the largest, external spheroid thus corresponding to the value $f = 1$. The semi-lengths of the major and minor axes of the f -spheroid are thus denoted a_f and b_f , and are related to f through the relation

$$f = \frac{a_f b_f^2}{a_1 b_1^2}. \quad (1)$$

The common focal distance c of all spheroids is given by

$$c = \sqrt{a_f^2 - b_f^2} = \sqrt{a_1^2 - b_1^2} \quad (\forall f), \quad (2)$$

and the eccentricities of the f -spheroid and the outer one are defined by

$$e_f = \frac{c}{a_f} \quad ; \quad e_1 = \frac{c}{a_1}. \quad (3)$$

From equations (1), (2) and (3), one may establish the following relation between f , e_f and e_1 :

$$f = \frac{e_1^3}{e_f^3} \frac{1 - e_f^2}{1 - e_1^2}, \quad (4)$$

which permits to determine the eccentricities e_f of all f -spheroids from that of the outer one, e_1 .

Use will be made of the following functions of the eccentricity e :

$$\alpha(e) = \frac{1 - e^2}{e^3} \arg \tanh e - \frac{1 - e^2}{e^2} \quad ; \quad \beta(e) = -\frac{1 - 3\alpha(e)}{e^2}; \quad (5)$$

the values of these functions on the internal and external spheroids will be logically denoted α_f , β_f , α_1 , β_1 . The notation

$$\gamma_f = \alpha_f - \frac{1 - e_f^2}{3 - e_f^2} \quad (6)$$

will also be employed to lighten some expressions.

2.2 The prolate spheroidal voided representative element

We now consider (Fig. 3) a prolate spheroidal representative volume element (RVE) containing a prolate spheroidal void. The entire domain is denoted Ω , the shell of material lying between the inner and outer spheroids Ω_M , and the void Ω_D .¹ The porosity is $f = \frac{\text{vol}\Omega_D}{\text{vol}\Omega}$. On the outer boundary $\partial\Omega$, a single unit normal vector \mathbf{n} , oriented outwards, is considered. On the inner boundary $\partial\Omega_D$, two unit normal vectors are considered, \mathbf{n}^+ oriented toward the exterior of Ω_D , and $\mathbf{n}^- = -\mathbf{n}^+$ oriented toward the exterior of Ω_M .

¹ The notations Ω_M and Ω_D are logical insofar as in the application to transformation plasticity, the material domain will be occupied by the mother-phase (M) and the void by the daughter-phase (D).

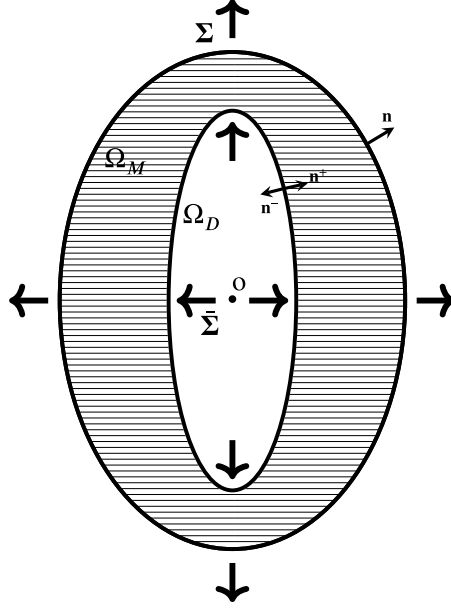


Fig. 3. The prolate spheroidal representative volume element.

The outer and inner boundaries of the material domain Ω_M , identical to $\partial\Omega$ and $\partial\Omega_D$, are subjected to conditions of homogeneous stress, as defined by Mandel (1964) and Hill (1967):

$$\begin{cases} \boldsymbol{\sigma}(\mathbf{x}) \cdot \mathbf{n}(\mathbf{x}) = \boldsymbol{\Sigma} \cdot \mathbf{n}(\mathbf{x}) & \text{on } \partial\Omega \\ \boldsymbol{\sigma}(\mathbf{x}) \cdot \mathbf{n}^-(\mathbf{x}) = -\bar{\boldsymbol{\Sigma}} \cdot \mathbf{n}^-(\mathbf{x}) & \text{on } \partial\Omega_D. \end{cases} \quad (7)$$

In these equations the symmetric second-rank tensors $\boldsymbol{\Sigma}$ and $\bar{\boldsymbol{\Sigma}}$ represent the “macroscopic stress” applied onto the RVE on the one hand, and the “internal loading” on the other hand.² There are no body forces.

For any displacement field $\mathbf{u}(\mathbf{x})$ defined over Ω_M and extended smoothly but otherwise arbitrarily over Ω_D , we define the “overall external and internal strain tensors” \mathbf{E} , $\bar{\mathbf{E}}$ by the formulae

$$\mathbf{E} \equiv \langle \boldsymbol{\epsilon}(\mathbf{u}) \rangle_{\Omega} \quad ; \quad \bar{\mathbf{E}} \equiv \langle \boldsymbol{\epsilon}(\mathbf{u}) \rangle_{\Omega_D}. \quad (8)$$

By Green’s theorem, the components of \mathbf{E} and $\bar{\mathbf{E}}$ may equivalently be written as

$$E_{ij} = \frac{1}{\text{vol}(\Omega)} \int_{\partial\Omega} \frac{1}{2} (u_i n_j + u_j n_i) dS \quad ; \quad \bar{E}_{ij} = \frac{1}{\text{vol}(\Omega_D)} \int_{\partial\Omega_D} \frac{1}{2} (u_i n_j^+ + u_j n_i^+) dS, \quad (9)$$

which clearly shows that the values of \mathbf{E} and $\bar{\mathbf{E}}$ are the same no matter how the displacement field is extended over Ω_D .

² A minus sign is conventionally introduced in equation (7)₂ so as to produce more natural-looking expressions in the sequel.

With the boundary conditions (7), the virtual power \mathcal{P}_e of external forces is given by

$$\begin{aligned}\mathcal{P}_e &\equiv \int_{\partial\Omega} \sigma_{ij} n_j \dot{u}_i dS + \int_{\partial\Omega_D} \sigma_{ij} n_j^- \dot{u}_i dS = \int_{\partial\Omega} \Sigma_{ij} n_j \dot{u}_i dS + \int_{\partial\Omega_D} \bar{\Sigma}_{ij} n_j^+ \dot{u}_i dS \\ &= \Sigma_{ij} \int_{\partial\Omega} \frac{1}{2} (\dot{u}_i n_j + \dot{u}_j n_i) dS + \bar{\Sigma}_{ij} \int_{\partial\Omega_D} \frac{1}{2} (\dot{u}_i n_j^+ + \dot{u}_j n_i^+) dS,\end{aligned}$$

or equivalently by equations (9) and the definition of the porosity f :

$$\mathcal{P}_e = \text{vol}(\Omega) \Sigma_{ij} \dot{E}_{ij} + \text{vol}(\Omega_D) \bar{\Sigma}_{ij} \dot{\bar{E}}_{ij} = \text{vol}(\Omega) (\boldsymbol{\Sigma} : \dot{\mathbf{E}} + f \bar{\boldsymbol{\Sigma}} : \dot{\bar{\mathbf{E}}}). \quad (10)$$

2.3 Number and choice of trial displacement fields

We shall consider only axisymmetric problems, for which the components of the overall stress and strain tensors are of the form

$$\begin{cases} \Sigma_{11} = \Sigma_{22} \equiv \Sigma_1 \neq 0 ; \Sigma_{33} \equiv \Sigma_3 \neq 0 ; \text{other } \Sigma_{ij} = 0 \\ \bar{\Sigma}_{11} = \bar{\Sigma}_{22} \equiv \bar{\Sigma}_1 \neq 0 ; \bar{\Sigma}_{33} \equiv \bar{\Sigma}_3 \neq 0 ; \text{other } \bar{\Sigma}_{ij} = 0 \\ E_{11} = E_{22} \equiv E_1 \neq 0 ; E_{33} \equiv E_3 \neq 0 ; \text{other } E_{ij} = 0 \\ \bar{E}_{11} = \bar{E}_{22} \equiv \bar{E}_1 \neq 0 ; \bar{E}_{33} \equiv \bar{E}_3 \neq 0 ; \text{other } \bar{E}_{ij} = 0. \end{cases} \quad (11)$$

The problem thus involves 4 kinematic parameters E_1 , E_3 , \bar{E}_1 and \bar{E}_3 . But in the limit-analysis to follow, the material in the domain Ω_M will be considered as incompressible; this entails the following relation between kinematic parameters:

$$\text{tr } \mathbf{E} = 2E_1 + E_3 = f \text{tr } \bar{\mathbf{E}} = f(2\bar{E}_1 + \bar{E}_3). \quad (12)$$

Thus there are only 3 independent kinematic parameters, implying that at least 3 independent incompressible trial displacement fields are required.

Like in our previous work on transformation plasticity assuming growing nuclei of daughter-phase of spherical shape (El Majaty *et al.*, 2018), we shall exploit an analogy with the problem of a prolate spheroidal RVE containing a confocal spheroidal *traction-free* void. The additional internal loading considered here is of no consequence upon the space of kinematically admissible, incompressible displacement fields adapted to the problem. The difference with our previous work (El Majaty *et al.*, 2018) is that we shall use, instead of the limit-analysis of a hollow *sphere* of Monchiet *et al.* (2011), the later work of the same authors on a hollow *spheroid* (Monchiet *et al.*, 2014).

The trial displacement fields employed are detailed in Appendix A. They are three-fold:

- (1) The first, $\mathbf{u}^{(1)}$, depicts an incompressible expansion of the material domain.
- (2) The second, $\mathbf{u}^{(2)}$, corresponds to a uniform deviatoric straining of the RVE.

- (3) The third, $\mathbf{u}^{(3)}$, which first arose in the context of Eshelby (1957)'s seminal study of the ellipsoidal elastic inclusion problem, depicts a change of shape, without any expansion, of the spheroidal void.

The expressions of the components of the external and internal overall strain tensors $\mathbf{E}^{(i)}$, $\overline{\mathbf{E}}^{(i)}$ corresponding to these displacement fields are as follows:

$$\begin{cases} E_1^{(1)} = \frac{3}{2}(1 - \alpha_1) \\ E_3^{(1)} = 3\alpha_1 \end{cases} ; \begin{cases} \overline{E}_1^{(1)} = \frac{3}{2f}(1 - \alpha_f) \\ \overline{E}_3^{(1)} = \frac{3}{f}\alpha_f \end{cases} \quad (13)$$

$$\begin{cases} E_1^{(2)} = -\frac{1}{2} \\ E_3^{(2)} = 1 \end{cases} ; \begin{cases} \overline{E}_1^{(2)} = -\frac{1}{2} \\ \overline{E}_3^{(2)} = 1 \end{cases} \quad (14)$$

$$\begin{cases} E_1^{(3)} = \frac{3}{4}(-1 + \alpha_1 + \beta_1) \\ E_3^{(3)} = \frac{3}{2}(1 - \alpha_1 - \beta_1) \end{cases} ; \begin{cases} \overline{E}_1^{(3)} = \frac{3}{4f}(-1 + \alpha_f + \beta_f) \\ \overline{E}_3^{(3)} = \frac{3}{2f}(1 - \alpha_f - \beta_f) \end{cases} \quad (15)$$

Note that the fields $\mathbf{u}^{(2)}$ and $\mathbf{u}^{(3)}$ have $\text{tr } \mathbf{E}^{(2)} = \text{tr } \mathbf{E}^{(3)} = 0$; hence the volumetric strain of the RVE is to be described by the single field $\mathbf{u}^{(1)}$.

2.4 Conjugate parameters

We consider ‘‘general’’ incompressible trial displacement fields of the form

$$\mathbf{u}(\mathbf{x}) = q_1 \mathbf{u}^{(1)}(\mathbf{x}) + q_2 \mathbf{u}^{(2)}(\mathbf{x}) + q_3 \mathbf{u}^{(3)}(\mathbf{x}) \quad (16)$$

where q_1, q_2, q_3 are kinematic parameters. By equations (13), (14) and (15), the components of the corresponding external and internal overall strain tensors read:

$$\begin{cases} E_1 = \frac{3q_1}{2}(1 - \alpha_1) - \frac{q_2}{2} + \frac{3q_3}{4}(-1 + \alpha_1 + \beta_1) \\ E_3 = 3q_1\alpha_1 + q_2 + \frac{3q_3}{2}(1 - \alpha_1 - \beta_1) \\ \overline{E}_1 = \frac{3q_1}{2f}(1 - \alpha_f) - \frac{q_2}{2} + \frac{3q_3}{4f}(-1 + \alpha_f + \beta_f) \\ \overline{E}_3 = \frac{3q_1}{f}\alpha_f + q_2 + \frac{3q_3}{2f}(1 - \alpha_f - \beta_f) \end{cases} \quad (17)$$

The ‘‘conjugate’’ mechanical parameters Q_1, Q_2, Q_3 are defined through the equation $\mathcal{P}_e = Q_1 \dot{q}_1 + Q_2 \dot{q}_2 + Q_3 \dot{q}_3$ where \mathcal{P}_e denotes the virtual power of external forces like above. Combination of equations (10) and (17) then yields their expressions:

$$\begin{cases} \frac{Q_1}{\text{vol}(\Omega)} = 3(1 - \alpha_1)\Sigma_1 + 3\alpha_1\Sigma_3 + 3(1 - \alpha_f)\overline{\Sigma}_1 + 3\alpha_f\overline{\Sigma}_3 \\ \frac{Q_2}{\text{vol}(\Omega)} = -\Sigma_1 + \Sigma_3 - f\overline{\Sigma}_1 + f\overline{\Sigma}_3 \\ \frac{Q_3}{\text{vol}(\Omega)} = \frac{3}{2}(1 - \alpha_1 - \beta_1)(\Sigma_3 - \Sigma_1) + \frac{3}{2}(1 - \alpha_f - \beta_f)(\overline{\Sigma}_3 - \overline{\Sigma}_1). \end{cases} \quad (18)$$

2.5 Overall plastic dissipation

The material domain Ω_M is henceforward assumed to be made of a rigid-ideal-plastic medium (no elasticity, no strain hardening) obeying the von Mises criterion with yield stress $\bar{\sigma}_M$ and the associated flow rule. The local plastic dissipation is then defined as $\bar{\sigma}_M \dot{\epsilon}_{eq}$ where $\dot{\epsilon}_{eq} = (\frac{2}{3} \dot{\epsilon} : \dot{\epsilon})^{1/2}$ ($\dot{\epsilon}$ being the traceless strain rate tensor) denotes the von Mises equivalent strain rate. For any incompressible trial velocity field $\dot{\mathbf{u}}(\mathbf{x})$, defined as the time-derivative of a displacement field $\mathbf{u}(\mathbf{x})$ of type (16), the overall plastic dissipation \mathcal{D} is then, by definition,

$$\mathcal{D}(\dot{q}_1, \dot{q}_2, \dot{q}_3) = \int_{\Omega_M} \bar{\sigma}_M \dot{\epsilon}_{eq} d\Omega. \quad (19)$$

This dissipation being independent of the internal loading characterized by the tensor $\bar{\Sigma}$, its value is theoretically the same as in the case of a spheroidal cell containing a *traction-free* void, considered by Monchiet *et al.* (2014). We shall nevertheless use approximations slightly differing from those of these authors, for reasons explained in Appendix B where the calculations required are presented in some detail. The result reads as follows:

$$\frac{\mathcal{D}(\dot{q}_1, \dot{q}_2, \dot{q}_3)}{\text{vol}(\Omega)} \simeq \bar{\sigma}_M \int_f^1 [f^2 \dot{q}_2^2 + (2\mathcal{P}_{mm} \dot{q}_1^2 + \mathcal{P}_{dd} \dot{q}_3^2) u^2]^{1/2} \frac{du}{u^2} \quad (20)$$

where \mathcal{P}_{mm} and \mathcal{P}_{dd} are the diagonal components of a symmetric 2×2 matrix, given by

$$\begin{cases} \mathcal{P}_{mm} = 2 + \frac{f(1 - 3\alpha_1)^2 - (1 - 3\alpha_f)^2}{2(1 - f)} \\ \mathcal{P}_{dd} = \frac{3}{4(1 - f)} [f(1 - \alpha_1 - \beta_1)(1 - 3\alpha_1 - 3\beta_1) - (1 - \alpha_f - \beta_f)(1 - 3\alpha_f - 3\beta_f)] \\ \quad \times g(f, e_1) \end{cases} \quad (21)$$

where

$$\begin{aligned} g(f, e_1) &= 1 + 3f \left(1 - \frac{e_1^2}{e_f^2}\right) \left(1 - \frac{e_f^2}{e_1^2} \frac{1 - e_f^2}{1 - e_1^2}\right) \\ &\times \frac{\alpha_1(1 - 3\beta_1) - (1 - \beta_1)^2}{f(1 - \alpha_1 - \beta_1)(1 - 3\alpha_1 - 3\beta_1) - (1 - \alpha_f - \beta_f)(1 - 3\alpha_f - 3\beta_f)}. \end{aligned} \quad (22)$$

2.6 Overall yield criterion

From now on, the derivation of the overall yield criterion and flow rule basically follows the same lines as in our previous study of transformation plasticity for spherical nuclei of daughter-phase (El Majaty *et al.*, 2018), although detailed calculations are different and more complex; this warrants a shorter presentation.

According to the classical theory of limit-analysis (Hill, 1951), the *parametric* equations

of the overall yield locus, in the space of triplets of load parameters (Q_1, Q_2, Q_3) , read

$$Q_i = \frac{\partial \mathcal{D}}{\partial \dot{q}_i}(\dot{q}_1, \dot{q}_2, \dot{q}_3) \quad (i = 1, 2, 3) \quad (23)$$

where the \dot{q}_i 's act as parameters. The elimination of these parameters between the expressions of Q_1, Q_2, Q_3 , if possible, then leads to the *explicit* equation of the overall yield locus, $\Phi(Q_1, Q_2, Q_3) = 0$.

This elimination is achieved with the aid of the so-called Gurson's lemma, the simplest presentation and proof of which is to be found in (Madou and Leblond, 2012):

Gurson's lemma. *Consider the integral*

$$J(p, q) = \int_{u_1}^{u_2} \sqrt{p^2 + q^2 u^2} \frac{du}{u^2} \quad (24)$$

where u_1 and u_2 are given positive bounds. Then the derivatives $\partial J/\partial p$ and $\partial J/\partial q$ are connected through the relation (where p and q no longer appear):

$$\left(\frac{\partial J}{\partial p}\right)^2 + \frac{2}{u_1 u_2} \cosh\left(\frac{\partial J}{\partial q}\right) - \frac{1}{u_1^2} - \frac{1}{u_2^2} = 0. \quad (25)$$

Applied to equation (20) with $u_1 = f$, $u_2 = 1$, $p = f\dot{q}_2$, $q = \sqrt{2\mathcal{P}_{mm}\dot{q}_1^2 + \mathcal{P}_{dd}\dot{q}_3^2}$, $J(p, q) = \frac{\mathcal{D}(\dot{q}_1, \dot{q}_2, \dot{q}_3)}{\text{vol}(\Omega)\bar{\sigma}_M}$, this lemma yields

$$\left(\frac{\partial \mathcal{D}/\partial p}{\text{vol}(\Omega)\bar{\sigma}_M}\right)^2 + \frac{2}{f} \cosh\left(\frac{\partial \mathcal{D}/\partial q}{\text{vol}(\Omega)\bar{\sigma}_M}\right) - \frac{1}{f^2} - 1 = 0. \quad (26)$$

The rest consists of somewhat heavy but straightforward calculations. One must first relate $\partial \mathcal{D}/\partial p$ and $\partial \mathcal{D}/\partial q$ to the derivatives $\partial \mathcal{D}/\partial \dot{q}_1$, $\partial \mathcal{D}/\partial \dot{q}_2$, $\partial \mathcal{D}/\partial \dot{q}_3$ using the expressions of p and q , then substitute the mechanical parameters Q_1, Q_2, Q_3 for these derivatives using equation (23), and finally use equations (18) to express these parameters in terms of overall stress components.

The criterion $\Phi(Q_1, Q_2, Q_3) = 0$ obtained in this way involves somewhat complex linear combinations of overall stress components. These expressions may however be put into a more appealing format by introducing the following definitions:

$$\begin{cases} \mathbf{X}_f = \frac{3}{2}(1 - \alpha_f)(\mathbf{e}_1 \otimes \mathbf{e}_1 + \mathbf{e}_2 \otimes \mathbf{e}_2) + 3\alpha_f \mathbf{e}_3 \otimes \mathbf{e}_3 \\ \mathbf{X}_1 = \frac{3}{2}(1 - \alpha_1)(\mathbf{e}_1 \otimes \mathbf{e}_1 + \mathbf{e}_2 \otimes \mathbf{e}_2) + 3\alpha_1 \mathbf{e}_3 \otimes \mathbf{e}_3 \end{cases} ; \quad S = \boldsymbol{\Sigma} : \mathbf{X}_1 + \bar{\boldsymbol{\Sigma}} : \mathbf{X}_f \quad (27)$$

$$\begin{cases} \mathbf{T} = \boldsymbol{\Sigma} + f\bar{\boldsymbol{\Sigma}} \\ \tilde{\mathbf{T}} = \frac{3}{2}(1 - \alpha_1 - \beta_1)\boldsymbol{\Sigma} + \frac{3}{2}(1 - \alpha_f - \beta_f)\bar{\boldsymbol{\Sigma}} \end{cases} ; \quad S_H = \left(\frac{S^2}{2\mathcal{P}_{mm}} + \frac{\tilde{T}_{eq}^2}{\mathcal{P}_{dd}}\right)^{1/2} ; \quad (28)$$

note that by equations (18), the quantities thus introduced are connected to the mechanical parameters Q_1, Q_2, Q_3 through the relations $S = \frac{Q_1}{\text{vol}(\Omega)}$, $T_{eq}^2 = \left(\frac{Q_2}{\text{vol}(\Omega)}\right)^2$, $\tilde{T}_{eq}^2 = \left(\frac{Q_3}{\text{vol}(\Omega)}\right)^2$.

The quantities $T_{eq} \equiv \left(\frac{3}{2}\mathbf{T}' : \mathbf{T}'\right)^{1/2}$, $\tilde{T}_{eq} \equiv \left(\frac{3}{2}\tilde{\mathbf{T}}' : \tilde{\mathbf{T}}'\right)^{1/2}$ (\mathbf{T}' , $\tilde{\mathbf{T}}'$: deviators of \mathbf{T} , $\tilde{\mathbf{T}}$) here denote the von Mises norms of the tensors \mathbf{T}' , $\tilde{\mathbf{T}}'$ in the sense of stresses.

With the notations introduced in equations (27) and (28), the overall yield criterion takes the following appealingly simple form:

$$\Phi(\boldsymbol{\Sigma}, \bar{\boldsymbol{\Sigma}}; f, e_1) = \frac{T_{eq}^2}{\bar{\sigma}_M^2} + 2f \cosh\left(\frac{S_H}{\bar{\sigma}_M}\right) - 1 - f^2 = 0. \quad (29)$$

Although this criterion has just been established for axisymmetric stress states only, it may be heuristically applied to general stress states using the definitions (27) and (28) of the quantities S , \mathbf{T} , $\tilde{\mathbf{T}}$ and S_H , of general scope. One should bear in mind, however, that such an extension of equation (29) to non-axisymmetric situations will inevitably entail some extra³ errors, owing to its purely phenomenological character.

2.7 Overall flow rule

We again follow here Hill (1951)'s classical approach of limit-analysis. We consider:

- a pair $(\boldsymbol{\Sigma}, \bar{\boldsymbol{\Sigma}})$ of overall external and internal stress tensors inducing a pair $(\dot{\mathbf{E}}, \dot{\bar{\mathbf{E}}})$ of overall external and internal strain rates, with $\boldsymbol{\sigma}(\mathbf{x})$ and $\dot{\boldsymbol{\epsilon}}(\mathbf{x})$ denoting the corresponding stress and strain rate fields;
- another pair $(\boldsymbol{\Sigma}^*, \bar{\boldsymbol{\Sigma}}^*)$ of plastically admissible overall external and internal stress tensors, with $\boldsymbol{\sigma}^*(\mathbf{x})$ denoting some stress field statically admissible with that pair and plastically admissible ($\sigma_{eq}^*(\mathbf{x}) \leq \bar{\sigma}_M$ everywhere in Ω_M).

Then, by equation (10) and the principle of virtual work,

$$\text{vol}(\Omega) \left[(\boldsymbol{\Sigma} - \boldsymbol{\Sigma}^*) : \dot{\mathbf{E}} + f(\bar{\boldsymbol{\Sigma}} - \bar{\boldsymbol{\Sigma}}^*) : \dot{\bar{\mathbf{E}}} \right] = \int_{\Omega_M} (\boldsymbol{\sigma} - \boldsymbol{\sigma}^*) : \dot{\boldsymbol{\epsilon}} d\Omega \geq 0$$

where the last inequality follows from the non-negativeness of the integrand here, a consequence of Hill's well-known principle in plasticity of metals. The geometric interpretation of this result is as follows: in the space of pairs $(\mathbf{W}, \bar{\mathbf{W}})$ of symmetric second-rank tensors, equipped with the Euclidian scalar product $(\mathbf{W}, \bar{\mathbf{W}}) \bullet (\mathbf{Z}, \bar{\mathbf{Z}}) \equiv \mathbf{W} : \mathbf{Z} + \bar{\mathbf{W}} : \bar{\mathbf{Z}}$, the scalar product of the pairs $(\boldsymbol{\Sigma} - \boldsymbol{\Sigma}^*, \bar{\boldsymbol{\Sigma}} - \bar{\boldsymbol{\Sigma}}^*)$ and $(\dot{\mathbf{E}}, f\dot{\bar{\mathbf{E}}})$ is non-negative whatever the plastically admissible pairs $(\boldsymbol{\Sigma}^*, \bar{\boldsymbol{\Sigma}}^*)$. This entails, following a classical reasoning, that the pair $(\dot{\mathbf{E}}, f\dot{\bar{\mathbf{E}}})$ is orthogonal (in the sense of the scalar product \bullet) to the yield locus at the "point" $(\boldsymbol{\Sigma}, \bar{\boldsymbol{\Sigma}})$, and directed outwards; hence there exists a non-negative scalar $\dot{\Lambda}$ - the *overall plastic multiplier* - such that

$$\dot{\mathbf{E}} = \dot{\Lambda} \frac{\partial \Phi}{\partial \boldsymbol{\Sigma}}(\boldsymbol{\Sigma}, \bar{\boldsymbol{\Sigma}}, f) \quad ; \quad f\dot{\bar{\mathbf{E}}} = \dot{\Lambda} \frac{\partial \Phi}{\partial \bar{\boldsymbol{\Sigma}}}(\boldsymbol{\Sigma}, \bar{\boldsymbol{\Sigma}}, f). \quad (30)$$

³ *Extra* because even in the axisymmetric case, the procedure of derivation involved various approximations, as was seen above.

Evaluating the derivatives here using equations (27), (28) and (29), we get the overall flow rule in its final form:

$$\left\{ \begin{array}{l} \dot{\mathbf{E}} = \frac{\dot{\Lambda}}{\bar{\sigma}_M^2} \left\{ 3\mathbf{T}' + f \frac{\sinh(S_H/\bar{\sigma}_M)}{S_H/\bar{\sigma}_M} \left[\frac{S}{\mathcal{P}_{mm}} \mathbf{X}_1 + \frac{9}{2\mathcal{P}_{dd}} (1 - \alpha_1 - \beta_1) \tilde{\mathbf{T}}' \right] \right\} \\ \dot{\tilde{\mathbf{E}}} = \frac{\dot{\Lambda}}{\bar{\sigma}_M^2} \left\{ 3\mathbf{T}' + \frac{\sinh(S_H/\bar{\sigma}_M)}{S_H/\bar{\sigma}_M} \left[\frac{S}{\mathcal{P}_{mm}} \mathbf{X}_f + \frac{9}{2\mathcal{P}_{dd}} (1 - \alpha_f - \beta_f) \tilde{\mathbf{T}}' \right] \right\} \end{array} \right. , \quad \dot{\Lambda} \geq 0. \quad (31)$$

where again a prime denotes a deviator.

3 Application to transformation plasticity

3.1 Geometric preliminaries

A few complements now become necessary with regard to the prolate spheroidal geometry introduced in Subsection 2.1.

First we introduce classical prolate spheroidal coordinates (λ, ψ, ϕ) , defined through their relations with the Cartesian coordinates (x_1, x_2, x_3) :

$$\begin{cases} x_1 = c \sinh \lambda \sin \psi \cos \phi \\ x_2 = c \sinh \lambda \sin \psi \sin \phi \\ x_3 = c \cosh \lambda \cos \psi \end{cases} \quad (32)$$

where c is the common focal distance of confocal spheroids, introduced in equation (2). The coordinates λ , ψ and ϕ play the same respective roles for the spheroidal geometry as the distance to the origin, the polar angle and the azimuthal angle for the spherical geometry. They are ‘‘orthogonal’’ in the sense that the tangent vectors $\partial \mathbf{x} / \partial \lambda$, $\partial \mathbf{x} / \partial \psi$, $\partial \mathbf{x} / \partial \phi$ to the coordinate lines form an orthogonal (but not orthonormal!) basis. The iso- λ surfaces are prolate confocal spheroids of major and minor semi-axes $a = c \cosh \lambda$ and $b = c \sinh \lambda$, respectively.

One immediately gets the vector $\partial \mathbf{x} / \partial \lambda$ from the definition (32):

$$\frac{\partial \mathbf{x}}{\partial \lambda} = c \cosh \lambda \sin \psi (\cos \phi \mathbf{e}_1 + \sin \phi \mathbf{e}_2) + c \sinh \lambda \cos \psi \mathbf{e}_3. \quad (33)$$

This vector is locally orthogonal to the confocal spheroid of parameter λ , but its norm differs from unity:

$$\begin{aligned} \left\| \frac{\partial \mathbf{x}}{\partial \lambda} \right\| &= c (\cosh^2 \lambda \sin^2 \psi \cos^2 \phi + \cosh^2 \lambda \sin^2 \psi \sin^2 \phi + \sinh^2 \lambda \cos^2 \psi)^{1/2} \\ &= c (\cosh^2 \lambda - \cos^2 \psi)^{1/2}; \end{aligned} \quad (34)$$

the unit vector \mathbf{e}_λ positively collinear to $\partial\mathbf{x}/\partial\lambda$ is therefore given by

$$\mathbf{e}_\lambda = \frac{\partial\mathbf{x}/\partial\lambda}{\|\partial\mathbf{x}/\partial\lambda\|} = \frac{\cosh \lambda \sin \psi (\cos \phi \mathbf{e}_1 + \sin \phi \mathbf{e}_2) + \sinh \lambda \cos \psi \mathbf{e}_3}{(\cosh^2 \lambda - \cos^2 \psi)^{1/2}}. \quad (35)$$

Now consider two infinitesimally close confocal spheroids of parameters λ and $\lambda + \delta\lambda$. The infinitesimal thickness δh of the layer lying between these spheroids, measured perpendicularly to them, is obviously

$$\delta h = \left\| \frac{\partial\mathbf{x}}{\partial\lambda} \right\| \delta\lambda = c(\cosh^2 \lambda - \cos^2 \psi)^{1/2} \delta\lambda. \quad (36)$$

Note that this thickness is not uniform over the spheroid (unlike that between concentric spheres).

Finally let λ_f and λ_1 denote, like in Subsection 2.1 and subsequent ones, the values of the parameter λ on the innermost and outermost spheroids. By equation (1), the ratio f of the volumes of these spheroids is given by

$$f = \frac{\cosh \lambda_f \sinh^2 \lambda_f}{\cosh \lambda_1 \sinh^2 \lambda_1}. \quad (37)$$

3.2 Principle of the treatment

For feasibility of the mathematical treatment, we introduce the hypothesis that *the growing nucleus of daughter-phase assumes the shape of increasing confocal spheroids*. (Assuming *homothetical* growth of this nucleus would admittedly be more natural, but lead to intractable algebraic complications. The effect of the variation in time of the shape of the growing nucleus will be evoked in Subsection 4.1 below).

With this hypothesis, the principle of the treatment is basically the same as in the case of a growing nucleus of daughter-phase of *spherical* shape (El Majaty *et al.*, 2018). We represent an elementary volume in a metal or alloy, undergoing some solid-solid phase transformation under stress, by the spheroidal RVE presented in Subsection 2.2. This RVE is subjected not only to some given external stress Σ , but also to some internal strain rate $\dot{\mathbf{E}}$ resulting from the expansion of the growing core of daughter-phase.

The problem to be solved is as follows:

- The given data include the external stress tensor Σ and the internal strain rate tensor $\dot{\mathbf{E}}$ imposed by the transformation - the calculation of which is presented in Subsection 3.3 below.
- The unknowns to be determined are the internal stress tensor $\bar{\Sigma}$, the overall strain rate $\dot{\mathbf{E}}$ and the plastic multiplier $\dot{\Lambda}$; but among these, one should distinguish between $\dot{\mathbf{E}}$, which is the true quantity of interest, and $\bar{\Sigma}$ and $\dot{\Lambda}$, which are mere ancillary unknowns to be eliminated.

- The equations to be used for the determination of the unknowns from the data are the overall yield criterion (29) and the double flow rule (31).

3.3 Calculation of the internal strain rate due to the transformation

The geometric and mechanical situation is depicted schematically in Fig. 4. At time t , the daughter-phase occupies the interior of the spheroid of parameter λ_f . Between times t and $t + \delta t$, the layer between the spheroids of parameters λ_f and $\lambda_f + \delta\lambda_f$ transforms from the mother- to the daughter-phase; thus at time $t + \delta t$ the daughter-phase occupies the interior of the spheroid of parameter $\lambda_f + \delta\lambda_f$. Because of the volume change accompanying the transformation, the spheroid of parameter $\lambda_f + \delta\lambda_f$ moves between times t and $t + \delta t$ by the amount δu_λ in the direction of the unit vector \mathbf{e}_λ - thus generating some microplasticity in the surrounding mother-phase, responsible for transformation plasticity in Greenwood and Johnson (1965)'s interpretation of the phenomenon.

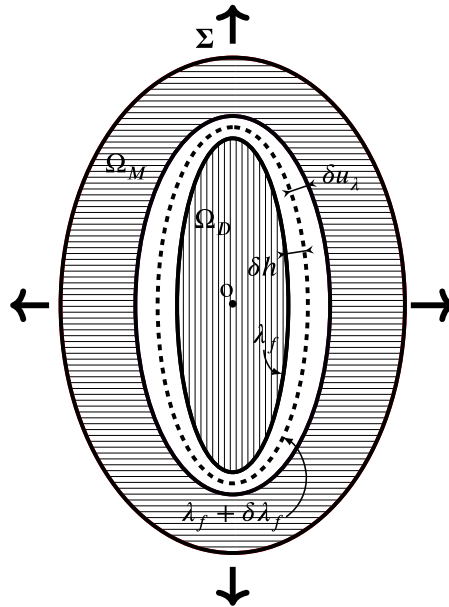


Fig. 4. Growth of a prolate spheroidal nucleus of daughter-phase within a confocal spheroidal domain of mother-phase.

The first task is to relate the increase $\delta\lambda_f$ of the parameter λ_f , characterizing the boundary of the spheroidal domain of daughter-phase, to the increase δf of the volume fraction f of this phase. This is easily done through differentiation of equation (37) with respect to time (at fixed parameter λ_1):

$$\delta f = \frac{(3 \cosh^2 \lambda_f - 1) \sinh \lambda_f}{\cosh \lambda_1 \sinh^2 \lambda_1} \delta \lambda_f. \quad (38)$$

Now consider (Fig. 5) some elementary domain within the layer transformed between times t and $t + \delta t$, located around the point of coordinates (λ_f, ψ, ϕ) . At time t , the volume of this domain is $\delta S \delta h$, where δS is the elementary area on the spheroid of

parameter λ_f , and δh the local elementary thickness given by equation (36) with λ_f and $\delta\lambda_f$ instead of λ and $\delta\lambda$. At time $t + \delta t$, this volume has become $\delta S(\delta h + \delta u_\lambda)$, since the thickness has increased by δu_λ . But neglecting the elastic volumetric strain of the daughter-phase, this final volume also amounts to $\delta S \delta h (1 + \frac{\Delta V}{V})$ where $\frac{\Delta V}{V}$ denotes the (known) relative variation of specific volume from the mother- to the daughter-phase (hereafter termed “volumetric transformation strain” for brevity). Identity of these two expressions demands that

$$\delta u_\lambda = \frac{\Delta V}{V} \delta h = \frac{\Delta V}{V} c (\cosh^2 \lambda_f - \cos^2 \psi)^{1/2} \delta \lambda_f \quad (39)$$

where equation (36) has been used.

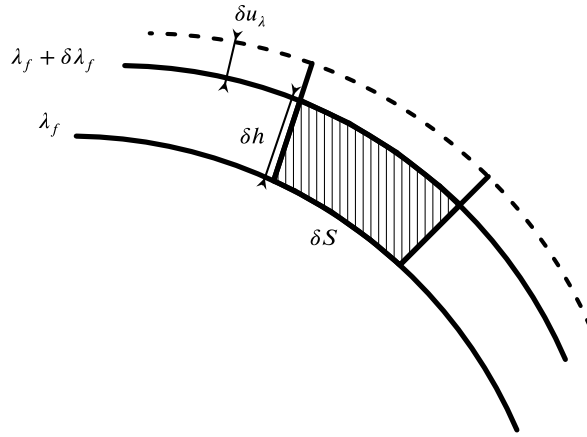


Fig. 5. Transformation of an elementary domain enclosed between the spheroids of parameters λ_f and $\lambda_f + \delta\lambda_f$.

One must now calculate the increment $\delta\bar{\mathbf{E}}$ of internal strain corresponding to the increment of displacement δu_λ given by equation (39). The calculation is made much easier by the remark that such a δu_λ is generated by an increment of displacement $\delta\mathbf{u}(\mathbf{x})$ of the form

$$\delta\mathbf{u}(\mathbf{x}) = \delta\bar{\mathbf{E}} \cdot \mathbf{x} = \delta\bar{E}_1(x_1\mathbf{e}_1 + x_2\mathbf{e}_2) + \delta\bar{E}_3x_3\mathbf{e}_3 \quad (\forall \mathbf{x} \in \partial\Omega_D) \quad (40)$$

for some values of $\delta\bar{E}_1$ and $\delta\bar{E}_3$; this indeed permits to circumvent the calculation of integrals in equation (9)₂.⁴ To establish the property announced, calculate the component δu_λ of the vector $\delta\mathbf{u}$ given by equation (40) in the direction of the unit vector \mathbf{e}_λ :

$$\begin{aligned} \delta u_\lambda &= \delta\mathbf{u} \cdot \mathbf{e}_\lambda = \delta\bar{E}_1(x_1\mathbf{e}_1 \cdot \mathbf{e}_\lambda + x_2\mathbf{e}_2 \cdot \mathbf{e}_\lambda) + \delta\bar{E}_3x_3\mathbf{e}_3 \cdot \mathbf{e}_\lambda \\ &= c \frac{\delta\bar{E}_1 \cosh \lambda_f \sinh \lambda_f \sin^2 \psi + \delta\bar{E}_3 \cosh \lambda_f \sinh \lambda_f \cos^2 \psi}{(\cosh^2 \lambda_f - \cos^2 \psi)^{1/2}} \end{aligned} \quad (41)$$

where the definition (32) of spheroidal coordinates and the expression (35) of the vector \mathbf{e}_λ have been used. Coincidence of the two expressions (39) and (41) of δu_λ demands,

⁴ A classical, and easily proved result asserts that if equation (40) holds, then equation (9)₂ also holds (for the same value of $\delta\bar{\mathbf{E}}$).

upon multiplication by $(\cosh^2 \lambda_f - \cos^2 \psi)^{1/2}$, that

$$\frac{\Delta V}{V} (\cosh^2 \lambda_f - \cos^2 \psi) \delta \lambda_f = \delta \bar{E}_1 \cosh \lambda_f \sinh \lambda_f \sin^2 \psi + \delta \bar{E}_3 \cosh \lambda_f \sinh \lambda_f \cos^2 \psi$$

at every point of coordinates (λ_f, ψ, ϕ) on the spheroid of parameter λ_f . Such an identity is perfectly possible, since the dependence with respect to the position on the spheroid of parameter λ_f is of the same type (that is, $A \cos^2 \psi + B$) in both sides of the equality. Identifying thus terms proportional to $\cos^2 \psi$ and independent of ψ , one gets after a short calculation

$$\begin{cases} \delta \bar{E}_1 = \frac{\Delta V}{V} \coth \lambda_f \cdot \delta \lambda_f = \frac{\Delta V}{V} \coth \lambda_f \frac{\cosh \lambda_1 \sinh^2 \lambda_1}{(3 \cosh^2 \lambda_f - 1) \sinh \lambda_f} \delta f \\ \delta \bar{E}_3 = \frac{\Delta V}{V} \tanh \lambda_f \cdot \delta \lambda_f = \frac{\Delta V}{V} \tanh \lambda_f \frac{\cosh \lambda_1 \sinh^2 \lambda_1}{(3 \cosh^2 \lambda_f - 1) \sinh \lambda_f} \delta f \end{cases} \quad (42)$$

where equation (38) has been used.

These results may be put into a more appealing format by combining them in two different ways:

(1) first, note that

$$\begin{aligned} \text{tr } \delta \bar{\mathbf{E}} &= 2\delta \bar{E}_1 + \delta \bar{E}_3 = \frac{\Delta V}{V} (2 \coth \lambda_f + \tanh \lambda_f) \frac{\cosh \lambda_1 \sinh^2 \lambda_1}{(3 \cosh^2 \lambda_f - 1) \sinh \lambda_f} \delta f \\ &= \frac{\Delta V}{V} \frac{3 \cosh^2 \lambda_f - 1}{\cosh \lambda_f \sinh \lambda_f} \frac{\cosh \lambda_1 \sinh^2 \lambda_1}{(3 \cosh^2 \lambda_f - 1) \sinh \lambda_f} \delta f = \frac{\Delta V}{V} \frac{\delta f}{f} \end{aligned}$$

where equation (37) has been used;

(2) second, note also that

$$\frac{\delta \bar{E}_3}{\delta \bar{E}_1} = \tanh^2 \lambda_f = 1 - \frac{1}{\cosh^2 \lambda_f} = 1 - e_f^2$$

since $e_f = c/a_f = 1/\cosh \lambda_f$.

Thus equations (42) are equivalent (upon division by δt) to the system

$$\begin{cases} \text{tr } \dot{\bar{\mathbf{E}}} = 2\dot{\bar{E}}_1 + \dot{\bar{E}}_3 = \frac{\Delta V}{V} \frac{\dot{f}}{f} \\ (1 - e_f^2)\dot{\bar{E}}_1 - \dot{\bar{E}}_3 = 0 \end{cases} \quad (43)$$

which is simpler, and as a bonus eliminates all reference to the spheroidal coordinate λ_f - which will therefore no longer be needed in the sequel.

An interesting final remark pertains to the component of the displacement field $\delta \mathbf{u}(\mathbf{x})$ given by equation (40) along the direction of the ψ -coordinate line, proportional to the scalar product $\delta \mathbf{u} \cdot \frac{\partial \mathbf{x}}{\partial \psi}$. Using equations (32) and (40), one finds after a bit of calculation that this component is zero. This means that the field $\delta \mathbf{u}(\mathbf{x})$ given by equation (40) depicts,

between times t and $t + \delta t$, a purely *normal* extension, parallel to the vector \mathbf{e}_λ , of the layer lying between the spheroids of parameters λ_f and $\lambda_f + \delta\lambda_f$, without any shear strain.⁵ This further demonstrates the physical soundness of this field to describe the expansion of the layer during the transformation; indeed in the limit $\delta\lambda_f \rightarrow 0$, this expansion becomes analogous to the laterally constrained thermal dilation of a thin thermoelastic film bonded onto some rigid planar substrate, which occurs without any shear for obvious symmetry reasons.

3.4 Calculation of the transformation plastic strain rate for a zero external stress

For growth of a *spherical* nucleus of daughter-phase, the case of a zero external stress is devoid of interest, because in this case overall geometric and mechanical isotropy combined with incompressibility of plastic deformation implies that the transformation plastic strain must necessarily be zero. For growth of a *spheroidal* nucleus the situation is different because global isotropy is lost, and the non-vanishing of the transformation plastic strain under zero applied stress is a characteristic feature of the anisotropic mechanical behavior during the transformation (Desalos, 1981).

For $\boldsymbol{\Sigma} = \mathbf{0}$, the mechanical parameters defined in equations (27) and (28) take the values

$$S = \bar{\boldsymbol{\Sigma}} : \mathbf{X}_f; \quad \mathbf{T} = f\bar{\boldsymbol{\Sigma}}; \quad \tilde{\mathbf{T}} = \frac{3}{2}(1 - \alpha_f - \beta_f)\bar{\boldsymbol{\Sigma}}; \quad S_H = \left(\frac{S^2}{2\mathcal{P}_{mm}} + \frac{9}{4}(1 - \alpha_f - \beta_f)^2 \frac{\bar{\boldsymbol{\Sigma}}_{eq}^2}{\mathcal{P}_{dd}} \right)^{1/2}. \quad (44)$$

With these values the yield criterion (29) and the two-part flow rule (31) take the form

$$\left\{ \begin{array}{l} f^2 \frac{\bar{\boldsymbol{\Sigma}}_{eq}^2}{\bar{\sigma}_M^2} + 2f \cosh\left(\frac{S_H}{\bar{\sigma}_M}\right) - 1 - f^2 = 0 \\ \dot{\mathbf{E}} = \frac{\dot{\Lambda}}{\bar{\sigma}_M^2} \left\{ 3f\bar{\boldsymbol{\Sigma}}' + f \frac{\sinh(S_H/\bar{\sigma}_M)}{S_H/\bar{\sigma}_M} \left[\frac{S}{\mathcal{P}_{mm}} \mathbf{X}_1 + \frac{27}{4\mathcal{P}_{dd}}(1 - \alpha_1 - \beta_1)(1 - \alpha_f - \beta_f)\bar{\boldsymbol{\Sigma}}' \right] \right\} \\ \dot{\mathbf{E}} = \frac{\dot{\Lambda}}{\bar{\sigma}_M^2} \left\{ 3f\bar{\boldsymbol{\Sigma}}' + \frac{\sinh(S_H/\bar{\sigma}_M)}{S_H/\bar{\sigma}_M} \left[\frac{S}{\mathcal{P}_{mm}} \mathbf{X}_f + \frac{27}{4\mathcal{P}_{dd}}(1 - \alpha_f - \beta_f)^2 \bar{\boldsymbol{\Sigma}}' \right] \right\}. \end{array} \right. \quad (45)$$

The first task is to evaluate the internal stress state, that is the tensor $\bar{\boldsymbol{\Sigma}}$. This can be done in three steps. First, combination of eqns. (43)₂ and (45)₃ yields after some calculation

$$\bar{\Sigma}_1 - \bar{\Sigma}_3 = \frac{\gamma_f S / \mathcal{P}_{mm}}{\frac{2f}{3} \frac{S_H/\bar{\sigma}_M}{\sinh(S_H/\bar{\sigma}_M)} + \frac{3}{2\mathcal{P}_{dd}}(1 - \alpha_f - \beta_f)^2} \quad (46)$$

where the parameter γ_f has been defined in equation (6). Now this parameter has been checked numerically to always be positive, and S is positive as a consequence of combi-

⁵ The component of the field $\delta\mathbf{u}(\mathbf{x})$ along the direction of the ϕ -coordinate line is also trivially zero due to axisymmetry.

nation of equation (43)₁ (where $\frac{\Delta V}{V}$ is positive)⁶ and the trace of equation (45)₃. Hence equation (46) implies in particular that $\bar{\Sigma}_1 - \bar{\Sigma}_3$ is positive.

In a second step, with this result in mind, solving equation (45)₁ with respect to $\bar{\Sigma}_{eq} = \bar{\Sigma}_1 - \bar{\Sigma}_3$ yields:

$$\frac{\bar{\Sigma}_1 - \bar{\Sigma}_3}{\bar{\sigma}_M} = \sqrt{F\left(\frac{S_H}{\bar{\sigma}_M}\right)} \quad \text{where} \quad F(X) = \frac{1}{f^2} (1 + f^2 - 2f \cosh X). \quad (47)$$

Then combination of this result and equation (46) yields

$$\frac{S}{\bar{\sigma}_M} = \frac{\mathcal{P}_{mm}}{\gamma_f} \left[\frac{2f}{3} \frac{S_H/\bar{\sigma}_M}{\sinh(S_H/\bar{\sigma}_M)} + \frac{3}{2\mathcal{P}_{dd}} (1 - \alpha_f - \beta_f)^2 \right] \sqrt{F\left(\frac{S_H}{\bar{\sigma}_M}\right)}. \quad (48)$$

Finally in a third step, combination of equations (44)₄, (46) and (48) yields the following nonlinear equation on the sole unknown S_H :

$$\left(\frac{S_H}{\bar{\sigma}_M}\right)^2 = \left\{ \frac{9}{4\mathcal{P}_{dd}} (1 - \alpha_f - \beta_f)^2 + \frac{\mathcal{P}_{mm}}{2\gamma_f^2} \left[\frac{2f}{3} \frac{S_H/\bar{\sigma}_M}{\sinh(S_H/\bar{\sigma}_M)} + \frac{3}{2\mathcal{P}_{dd}} (1 - \alpha_f - \beta_f)^2 \right]^2 \right\} F\left(\frac{S_H}{\bar{\sigma}_M}\right). \quad (49)$$

Equation (49) on S_H may be solved numerically by various methods, the most robust (if not the quickest) of which is a simple dichotomy.⁷ Once this is done, $\bar{\Sigma}_1 - \bar{\Sigma}_3$ and S may be deduced from equations (47) and (48). Hence the internal stress state is entirely determined.

The second task is to determine the transformation plastic strain rate $\dot{\mathbf{E}}^{tp}$. First, we deduce the plastic multiplier $\dot{\Lambda}$ from combination of equation (43)₁ and the trace of equation (45)₃:

$$\frac{\dot{\Lambda}}{\bar{\sigma}_M^2} = \frac{1}{3} \frac{\Delta V}{V} \frac{\dot{f}}{f} \frac{S_H/\bar{\sigma}_M}{\sinh(S_H/\bar{\sigma}_M)} \frac{\mathcal{P}_{mm}}{S}. \quad (50)$$

We then insert this value into equation (45)₂ to get the external strain rate $\dot{\mathbf{E}}$. This “total” strain rate is composed of a hydrostatic part connected to the volumetric transformation strain $\frac{\Delta V}{V}$ and the transformation rate \dot{f} , plus a deviatoric part identical by definition to the transformation plastic strain rate $\dot{\mathbf{E}}^{tp}$:

$$\dot{\mathbf{E}} = \frac{1}{3} \frac{\Delta V}{V} \dot{f} \mathbf{1} + \dot{\mathbf{E}}^{tp}, \quad \text{tr } \dot{\mathbf{E}}^{tp} = 0 \quad \Rightarrow \quad \mathbf{E}(f) = \frac{1}{3} \frac{\Delta V}{V} f \mathbf{1} + \mathbf{E}^{tp}(f), \quad \text{tr } \mathbf{E}^{tp}(f) = 0 \quad (51)$$

where $\mathbf{E}(f)$ and $\mathbf{E}^{tp}(f)$ denote the total strain and transformation plastic strain resulting from transformation up to the fraction f of daughter-phase. It follows, upon some

⁶ This is true in practical situations of solid-solid transformations resulting from cooling during thermomechanical treatments.

⁷ Such a method is especially convenient in view of the fact that the possible interval of variation of the variable S_H , namely $|S_H| \leq \bar{\sigma}_M \ln \frac{1}{f}$, is known *a priori* from the criterion (29).

calculation, that the axial component of $\dot{\mathbf{E}}^{tp}$ amounts to

$$\dot{E}_3^{tp} = \dot{E}'_3 = \frac{\Delta V}{V} \dot{f} \left[\alpha_1 - \frac{1}{3} - \frac{2}{3} \frac{\mathcal{P}_{mm}}{S} (\bar{\Sigma}_1 - \bar{\Sigma}_3) \left(\frac{S_H/\bar{\sigma}_M}{\sinh(S_H/\bar{\sigma}_M)} + \frac{9}{4\mathcal{P}_{dd}} (1 - \alpha_1 - \beta_1)(1 - \alpha_f - \beta_f) \right) \right]. \quad (52)$$

The value of $E_3^{tp}(f = 1)$ after complete transformation may then be obtained from equation (52) through integration in time, for given values of the volumetric transformation strain $\frac{\Delta V}{V}$ and the eccentricity e_1 of the RVE.

Two special cases of equation (52) are of particular interest:

- (1) The *spherical* case in which the eccentricity e_1 of the RVE is zero; in this case $\alpha(e) = \frac{1}{3}$, $\beta(e) = \frac{2}{5}$, $\gamma_f = 0$ (see equations (5) and (6)), $\bar{\Sigma}_1 - \bar{\Sigma}_3 = 0$ (see equation (46)), so that $\dot{E}_3^{tp} = 0$. This result was to be expected in view of the overall isotropy of the geometry in this case, combined with incompressibility of plastic deformation.
- (2) The *cylindrical* case in which the eccentricity e_1 of the RVE is unity; in that case $\alpha(e) = 0$, $\beta(e) = 1$, $\gamma_f = 0$ (see equations (5) and (6)), $\bar{\Sigma}_1 - \bar{\Sigma}_3 = 0$ (see equation (46)), so that $\dot{E}_3^{tp} = -\frac{1}{3} \frac{\Delta V}{V} \dot{f}$ and $\dot{E}_3 = \frac{1}{3} \frac{\Delta V}{V} \dot{f} + \dot{E}_3^{tp} = 0$. Again, this last result, concerning now the *total* strain, could be expected in view of the rigid vertical constraint imposed at each step of the transformation by the previously transformed cylindrical core of daughter-phase. (This point is illustrated in Figs. 8(c) and 8(d) below, and discussed in more detail in Subsection 4.2).

Figure 6 illustrates the predictions of equation (52) by displaying the axial transformation plastic strain E_3^{tp} under zero external stress (obtained through integrating \dot{E}_3^{tp} in time) as a function of the volume fraction f of the daughter-phase (representing the progress of the transformation). The values (corresponding to the A508 Cl.3 steel around a temperature of 350°) of the material parameters are $\frac{\Delta V}{V} = 0.0252$ for the volumetric transformation strain and $\bar{\sigma}_M = 145$ MPa for the yield stress of the (γ) mother-phase⁸; and various possible eccentricities e_1 of the RVE are considered. Note in particular the values of $E_3^{tp}(f = 1)$ after complete transformation in the (almost) spherical and (almost) cylindrical cases, 0 and $-\frac{1}{3} \frac{\Delta V}{V} = -0.0084$ respectively, in agreement with what has just been said.

3.5 Calculation of the transformation plastic strain rate for a nonzero external stress

The calculation of $\dot{\mathbf{E}}^{tp}$ for an arbitrary external stress ($\boldsymbol{\Sigma} \neq \mathbf{0}$) is more involved but basically follows the same lines. We first define, for every symmetric second-rank tensor \mathbf{W} , a “modified deviator” $D\mathbf{W}$ by the formula

$$D\mathbf{W} = \mathbf{W} - \text{tr } \mathbf{W} \left[\frac{1}{3 - e_f^2} (\mathbf{e}_1 \otimes \mathbf{e}_1 + \mathbf{e}_2 \otimes \mathbf{e}_2) + \frac{1 - e_f^2}{3 - e_f^2} \mathbf{e}_3 \otimes \mathbf{e}_3 \right] \quad (53)$$

⁸ Note however that for the zero external stress envisaged here, \dot{E}_3^{tp} and E_3^{tp} are in fact independent of the value of $\bar{\sigma}_M$, as appears in equations (47)₁, (48), (49) and (52).

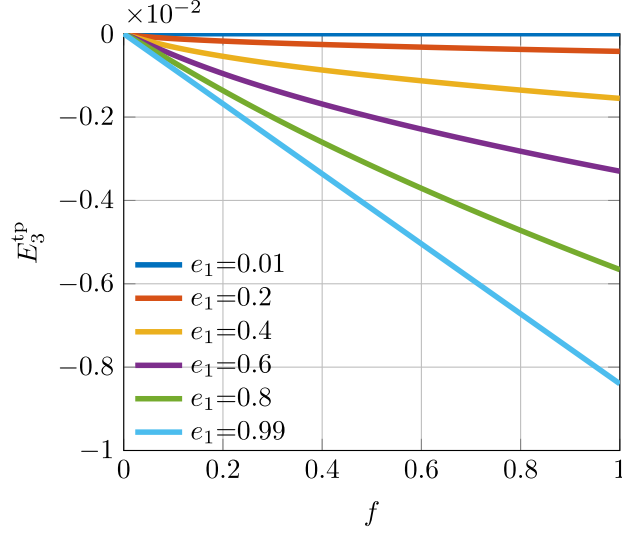


Fig. 6. Predicted axial transformation plastic strain E_3^{tp} versus volume fraction f of daughter-phase, in the absence of any stress applied, for various values of the RVE eccentricity e_1 .

(one immediately checks that $\text{tr } D\mathbf{W} = 0$). The advantage of this definition is that for an axisymmetric tensor (with sole possibly nonzero components $W_{11} = W_{22} = W_1$ and $W_{33} = W_3$), the relations $D\mathbf{W} = \mathbf{0}$ and $(1 - e_f^2)W_1 - W_3 = 0$ are equivalent; thus equation (43)₂ is equivalent to $D\dot{\mathbf{E}} = \mathbf{0}$.

Applying then the operator D to equation (31)₂, we then get, after some calculations, the internal stress deviator $\bar{\Sigma}'$ as a function of S and S_H :

$$\bar{\Sigma}' = \frac{1}{f \frac{S_H/\bar{\sigma}_M}{\sinh(S_H/\bar{\sigma}_M)} + \frac{9}{4\mathcal{P}_{dd}}(1 - \alpha_f - \beta_f)^2} \times \left\{ - \left[\frac{S_H/\bar{\sigma}_M}{\sinh(S_H/\bar{\sigma}_M)} + \frac{9}{4\mathcal{P}_{dd}}(1 - \alpha_1 - \beta_1)(1 - \alpha_f - \beta_f) \right] \Sigma' + \frac{\gamma_f S}{\mathcal{P}_{mm}} \left[\frac{1}{2}(\mathbf{e}_1 \otimes \mathbf{e}_1 + \mathbf{e}_2 \otimes \mathbf{e}_2) - \mathbf{e}_3 \otimes \mathbf{e}_3 \right] \right\}. \quad (54)$$

Combined with equations (28)_{1,2}, equation (54) permits to calculate T_{eq}^2 and \tilde{T}_{eq}^2 in terms of S and S_H . Two independent equations on the latter unknowns may then be obtained

- (1) from the yield criterion (29);
- (2) from the expression of S_H^2 deduced from the definition (28)₃ of S_H .

The resulting system of coupled nonlinear equations on S and S_H may be solved numerically by various methods, among which a simple one is sketched in Appendix C.

Once S_H , S and $\bar{\Sigma}'$ are known, one may calculate the plastic multiplier $\dot{\Lambda}$ by combining equation (43)₁ and the trace of equation (31)₂ (the result is equation (50), like in the absence of external stress); then the transformation plastic strain rate $\dot{\mathbf{E}}^{tp} = \dot{\mathbf{E}}'$ from

equation (31)₁. The final result reads

$$\dot{\mathbf{E}}^{tp} = \dot{\mathbf{E}}' = \frac{\Delta V}{V} \dot{f} \left[\frac{\mathcal{P}_{mm}}{fS} \frac{S_H/\bar{\sigma}_M}{\sinh(S_H/\bar{\sigma}_M)} \mathbf{T}' + \left(\frac{1}{3} \mathbf{X}'_1 + \frac{3\mathcal{P}_{mm}}{2S\mathcal{P}_{dd}} (1 - \alpha_1 - \beta_1) \tilde{\mathbf{T}}' \right) \right]. \quad (55)$$

Figure 7 illustrates the predictions of equation (55) in the same way (and for the same values of model parameters) as Figure 6, but now for various nonzero tensile and compressive axial external stresses.⁹

Several points are noteworthy here:

- In the spherical case ($e_1 = 0$), the predicted results are symmetric in tension and compression ($E_3^{tp}(-\Sigma) = -E_3^{tp}(\Sigma)$). Note also that the transformation plastic strain $E_3^{tp}(f = 1)$ after complete transformation increases nonlinearly with the stress applied, in agreement with various experimental results (see e.g. Greenwood and Johnson (1965)) and El Majaty *et al.* (2018)'s recent theoretical approach.
- In the cylindrical case ($e_1 = 0.9999 \simeq 1$), results in tension and compression are asymmetrical ($E_3^{tp}(-\Sigma) \neq -E_3^{tp}(\Sigma)$): indeed $E_3^{tp}(f = 1)$ *always takes the same value of* $-\frac{1}{3} \frac{\Delta V}{V} = -0.0084$ (corresponding to a total strain $E_3(f = 1) = 0$) *whatever the external stress applied*. Like in the case of a zero external stress, this seemingly paradoxical effect results from the rigid vertical constraint imposed by the previously transformed cylindrical core of daughter-phase, see Figs. 8(c) and 8(d) and Subsection 4.3.
- In some intermediary, spheroidal case ($e_1 = 0.8$), symmetry between tension and compression is lost like in the cylindrical case, but not to the point where $E_3^{tp}(f = 1)$ becomes independent of the stress applied.

Fundamentally, asymmetry between tension and compression (always present except in the special spherical case) arises from the definite (positive) sign of the volumetric transformation strain $\frac{\Delta V}{V}$.

4 Comparison with numerical FFT-based simulations

4.1 Principle of the simulations

In this Section, we present simulations, using an FFT-based numerical homogenization method (Moulinec and Suquet, 1998), of large RVEs containing numerous growing nuclei of daughter-phase. These simulations being similar in principle to those presented in our earlier work (El Majaty *et al.*, 2021)¹⁰ but for the different assumed shapes of the nuclei, a brief presentation will suffice.

⁹ Unlike for a zero external stress, the results now depend upon the value of the yield stress $\bar{\sigma}_M$ of the mother-phase.

¹⁰ Note that the prototype of such FFT-based simulations of transformation plasticity was presented by Otsuka *et al.* (2018), with a however somewhat different focus on crystal plasticity effects.

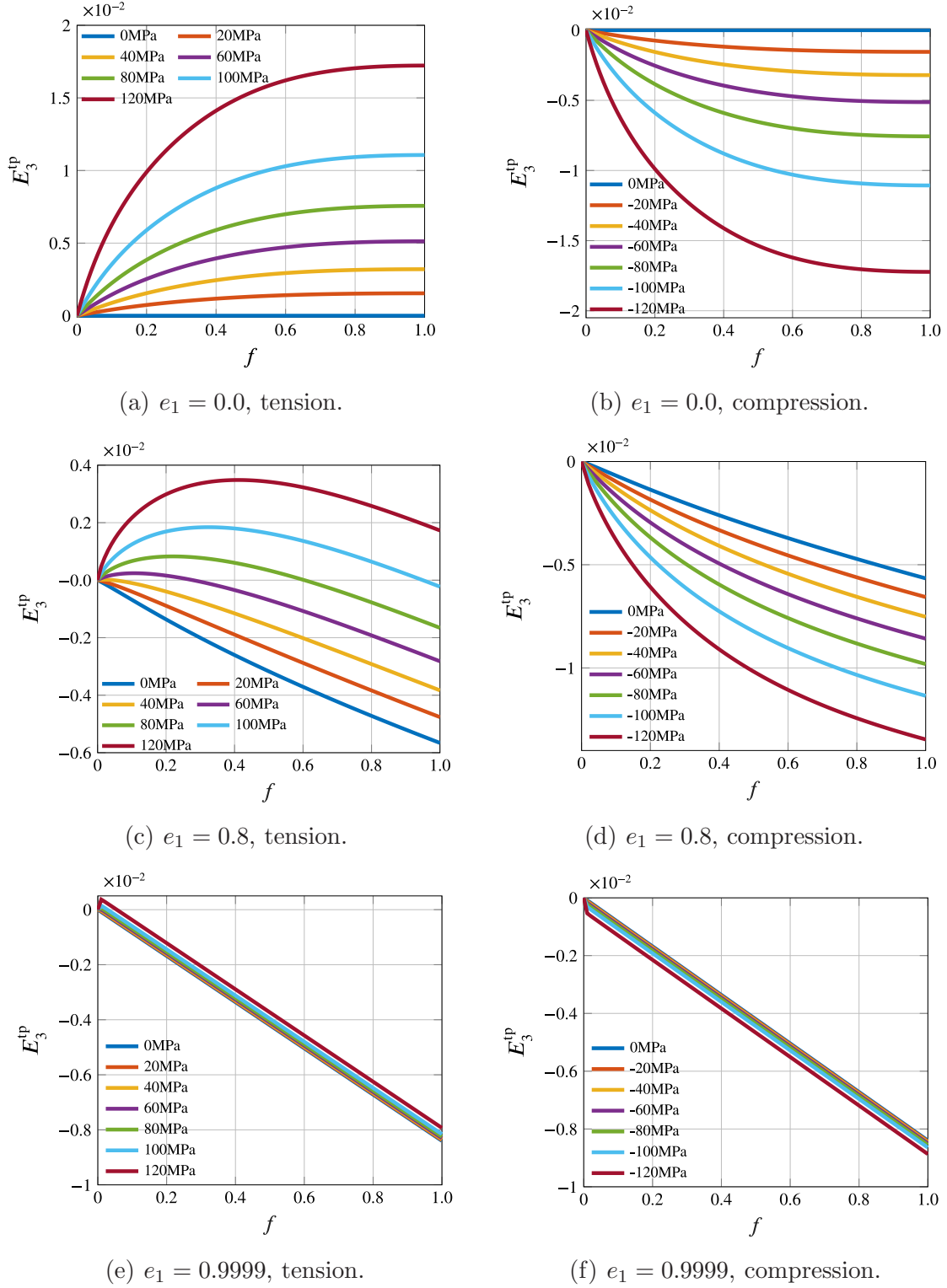


Fig. 7. Predicted axial transformation plastic strain E_3^{tp} versus volume fraction f of daughter-phase, under various tensile and compressive axial stresses applied, for various RVE eccentricities e_1 .

A parallelepipedic RVE (Fig. 8) subjected to periodic mechanical boundary conditions is discretized through some parallelepipedic lattice of $100 \times 100 \times 100$ voxels. (Such a large number of discretization points is much more efficiently dealt with the FFT-based method

than with the classical FE method). At each step of the calculation, each voxel is ascribed mechanical constants corresponding to one of the two phases: that is, Young's modulus and Poisson's ratio, 182 GPa and 0.3 for both phases; yield stress, 145 MPa for the (γ) mother-phase and 950 MPa for the (α) daughter-phase; initial inelastic strain (identical in all directions), 0 for the mother-phase and 0.0084 for the daughter-phase. (These constants correspond to the A 508 Cl.3 steel around 350°, like in Figs. 6 and 7 and our previous work (El Majaty *et al.*, 2021)).

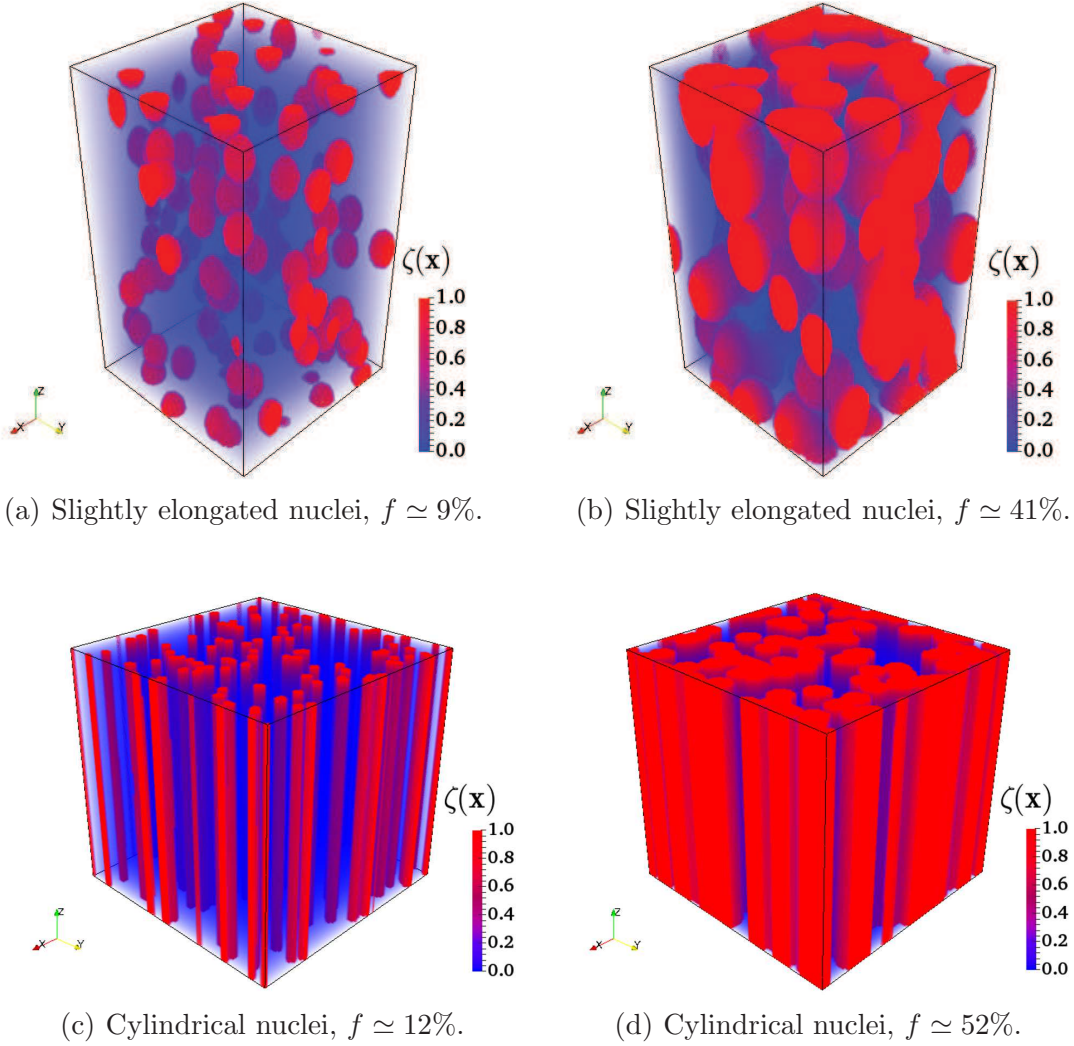


Fig. 8. Growth of spheroidal nuclei of daughter-phase within a RVE of mother-phase - (a) and (b): moderately elongated nuclei; (c) and (d): cylindrical nuclei.

The “transformation” at any point and instant simply corresponds to the imposed switch from one set of constants to the other,¹¹ which allows complete flexibility in the geometrical aspects of the transformation considered: absence vs. presence of continuous nucleation of new transformation sites (nucleation vs. growth), confocal vs. homothetical growth of

¹¹In fact, for numerical reasons of no interest here, the switch is imposed only gradually, using some control parameter ξ varying continuously between 0 (pure mother-phase) and 1 (pure daughter-phase); this explains the seemingly paradoxical gradual change of color from the mother- to the daughter-phase in Fig. 8.

pre-existing nuclei, etc. For instance, Fig. 8 illustrates two stages of the homothetical growth of moderately elongated or cylindrical nuclei present from the start of the transformation, in the absence of continuous nucleation of new ones. A detailed study of the influence of such features and similar ones upon transformation plasticity, not presented here for space reasons, has been performed, with the conclusion that their impact is small. We shall therefore be content with presenting only results corresponding to *homothetical* growth of *pre-existing* nuclei (no continuous nucleation of new transformation sites). The RVE considered will be a parallelepiped of dimensions proportional to the semi-axes of the nuclei, so as to well represent typical deformed elementary volumes in laminated plates (except for cylindrical nuclei for which considering an infinitely long cylinder would not only be impossible but pointless in view of axial translational invariance - a cubical RVE is considered in that case); see Fig. 8.

4.2 Case of a zero external stress: first elastic correction to the expression of $\dot{\mathbf{E}}^{tp}$

We first present numerical results obtained in the absence of external stress ($\Sigma = \mathbf{0}$). Exceptionally, in order to more clearly illustrate our comments, we do not plot in Fig. 9 the axial transformation plastic strain E_3^{tp} , but the *total* axial strain $E_3 = \frac{1}{3} \frac{\Delta V}{V} + E_3^{tp}$ obtained in the simulations, versus the fraction f of daughter-phase, for various RVE eccentricities e_1 .

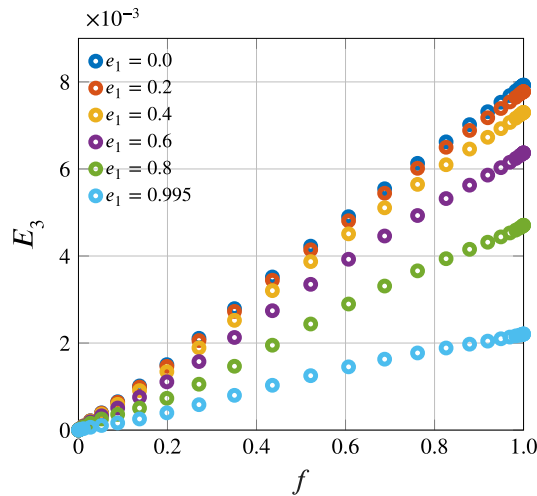


Fig. 9. Numerical total axial strain versus volume fraction of daughter-phase, for various values of the RVE eccentricity e_1 .

For *spherical* nuclei ($e_1 = 0$), the total strain $E_3(f = 1)$ after complete transformation amounts to 8×10^{-3} , just slightly less than the theoretical value of $\frac{1}{3} \frac{\Delta V}{V} + E_3^{tp}(f = 1) = \frac{1}{3} \frac{\Delta V}{V} = 8.4 \times 10^{-3}$. Such a small discrepancy is tolerable, all the more so since it certainly arises from some slight macroscopic anisotropy of the simulated RVE. For *cylindrical* nuclei ($e_1 = 0.995 \simeq 1$), however, the total strain $E_3(f = 1)$ after complete transformation amounts to 2.2×10^{-3} , which disagrees more markedly with the theoretical value of $\frac{1}{3} \frac{\Delta V}{V} + E_3^{tp}(f = 1) = \frac{1}{3} \frac{\Delta V}{V} - \frac{1}{3} \frac{\Delta V}{V} = 0$. Although the difference is not large, it

may be of some importance in the context of numerical predictions of residual stresses and distortions resulting from thermomechanical treatments, and should therefore be accounted for in a refined model of transformation plasticity.

The nonzero value of the axial final total strain for cylindrical nuclei clearly means that the effect of rigid vertical constraint imposed by the previously transformed cylinders of daughter-phase, already alluded to in Subsections 3.4 and 3.5, is not as absolute as predicted by the theory. This effect may be due to two possible causes:

- *Plasticity in the harder daughter-phase* (disregarded in the theory since the core of daughter-phase was considered not to deform after the transformation). But calculations with cylindrical nuclei have been performed with a value of the yield stress in the daughter-phase of 9,500 MPa instead of 950 MPa, thus eliminating any possibility of plastic straining of this phase, without any change in the results. The explanation of the effect therefore cannot lie there.
- *Presence of elasticity.* To test this possible cause, calculations with cylindrical nuclei have been performed with various values of the ratio $\bar{\sigma}_M/E$. Results showed that the smaller this ratio, that is the stiffer the material elastically, the closer to 0 the total strain $E_3(f = 1)$ after complete transformation. This unambiguously shows that *the origin of the effect lies in the presence of elasticity.*

It is not difficult to understand the mechanism by which, in the cylindrical case, elasticity somewhat influences transformation plasticity. Between times t and $t + \delta t$, when thin cylindrical shells of mother-phase are transformed into daughter-phase, and want to expand axially because of the volumetric transformation strain, their expansion is *not* completely hindered by the rigidity of the already existing cylinders of daughter-phase, but permitted to some extent by the elasticity of these cylinders. This phenomenon generates a slight increase of the plastic strain in the remaining mother-phase, which is later irreversibly transferred to the daughter-phase upon transformation; whence a slight increase, due to elasticity of the daughter-phase, of the axial transformation plastic strain and the total axial strain after complete transformation.

Unfortunately limit-analysis, the basis of the model developed here, considers only by definition loading states large enough for elasticity to become ineffective (see Drucker *et al.* (1952) and Leblond *et al.* (2018)). It cannot therefore account for the effects of this aspect of the mechanical behavior. Recent years have witnessed the development of sophisticated theories for homogenization of nonlinear materials including elasticity, but they have not yet reached a point where their results become explicit enough to be easily applied. This leaves only one possibility to account for the effect of elasticity upon Greenwood and Johnson (1965)'s mechanism of transformation plasticity, through some heuristic correction of the theoretical expression of $\dot{\mathbf{E}}^{tp}$.

Our proposal is to add to the expression $\dot{\mathbf{E}}^{tp \text{ theor}}$ of $\dot{\mathbf{E}}^{tp}$ provided by equation (55), an elastic correction given by

$$\dot{\mathbf{E}}^{corr1} = k_1 e_1^2 \frac{\Delta V}{V} \frac{\bar{\sigma}_M}{E} \dot{f} \left[-\frac{1}{2}(\mathbf{e}_1 \otimes \mathbf{e}_1 + \mathbf{e}_2 \otimes \mathbf{e}_2) + \mathbf{e}_3 \otimes \mathbf{e}_3 \right] \quad \text{with} \quad k_1 = 1.2 \times 10^2. \quad (56)$$

This proposed correction exhibits the following nice features:

- being proportional to e_1^2 , it is effective for cylindrical nuclei ($e_1 = 1$), as desired, but not for spherical nuclei ($e_1 = 0$), for which it is not needed;
- it is proportional to the volumetric transformation strain $\frac{\Delta V}{V}$, the source of Greenwood and Johnson (1965)'s mechanism of transformation plasticity;
- it is proportional to the ratio $\bar{\sigma}_M/E$, so as to be a decreasing function of the elastic stiffness;
- collinearity with the tensor $-\frac{1}{2}(\mathbf{e}_1 \otimes \mathbf{e}_1 + \mathbf{e}_2 \otimes \mathbf{e}_2) + \mathbf{e}_3 \otimes \mathbf{e}_3$ warrants both incompressibility and transverse isotropy with respect to the major axis of the nuclei;
- the parameter k_1 , being dimensionless (material constants are accounted for in other factors), may be expected to be material-independent.

With the material parameters considered in the example under discussion, the value of the axial component of the correction for cylindrical nuclei is, after complete transformation, 2.4×10^{-3} , corresponding to a total axial strain of $\frac{1}{3}\frac{\Delta V}{V} + E_3^{tp\ theor}(f=1) + E_3^{corr\ 1}(f=1) = \frac{1}{3}\frac{\Delta V}{V} - \frac{1}{3}\frac{\Delta V}{V} + 2.4 \times 10^{-3} = 2.4 \times 10^{-3}$, close to the value of 2.2×10^{-3} apparent in Fig. 9.¹²

4.3 Case of a nonzero external stress applied: second elastic correction to the expression of $\dot{\mathbf{E}}^{tp}$

Figure 10 now presents the axial transformation plastic strain E_3^{tp} obtained in the simulations versus the fraction f of daughter-phase, for an applied tensile axial stress Σ_3 of 80 MPa and various RVE eccentricities e_1 .

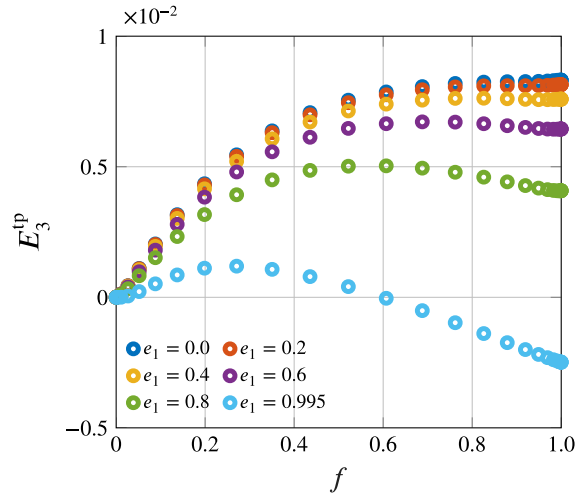


Fig. 10. Numerical axial transformation plastic strain versus volume fraction of daughter-phase, under a tensile axial stress of 80 MPa, for various values of the RVE eccentricity e_1 .

A fresh issue unfortunately arises again in the cylindrical case ($e_1 = 0.995 \simeq 1$). If the elastic correction $\dot{\mathbf{E}}^{corr\ 1}$ defined by equation (56) is not accounted for in the expression

¹² The slight discrepancy arises from the fact that all values of the RVE eccentricity e_1 , not just that corresponding to cylindrical nuclei, have been used for the fit of the value of k_1 .

of $\dot{\mathbf{E}}^{tp}$, the model value of $E_3^{tp}(f = 1)$ after complete transformation amounts to $-\frac{1}{3}\frac{\Delta V}{V} = -8.4 \times 10^{-3}$, in disagreement with the numerical value of -2.5×10^{-3} apparent in Fig. 10; no wonder here. But even if this correction is accounted for, the model value of $E_3^{tp}(f = 1)$ amounts to $-\frac{1}{3}\frac{\Delta V}{V} + E_3^{corr1} = -8.4 \times 10^{-3} + 2.4 \times 10^{-3} = -6 \times 10^{-3}$, which still disagrees with the numerical value.

Thus the elastic correction defined above in the absence of any external stress does not suffice. Again, it is not difficult to understand why. Referring to the discussion in Subsection 4.2, when thin cylindrical shells of mother-phase are transformed between times t and $t + \delta t$, the axial expansion of the RVE allowed by the elasticity of the already existing cylinders of daughter-phase depends upon the axial stress in these cylinders, and therefore upon the external stress. Hence the elastic correction of the transformation plastic strain rate, which is determined by the axial expansion of the RVE, *must* depend upon this external stress.

To account for this phenomenon, we propose to add to the expression $\dot{\mathbf{E}}^{tp\ theor}$ of $\dot{\mathbf{E}}^{tp}$ defined by equation (55), a second elastic correction now depending on Σ , given by

$$\dot{\mathbf{E}}^{corr2} = k_2 e_1 [1 + k_3 e_1 (1 - e_1)] \frac{\Delta V}{V} \frac{\Sigma_{eq}^2}{E \bar{\sigma}_M} (1 - f)^4 \dot{f} \cdot \frac{3 \Sigma'}{2 \Sigma_{eq}} \quad (57)$$

with $k_2 = 2.4 \times 10^3$ and $k_3 = 1.85$.

Some comments on this correction are again in order:

- being proportional to e_1 , it is again effective for cylindrical nuclei ($e_1 = 1$) but not for spherical nuclei ($e_1 = 0$) - as desired;
- it is again proportional to the volumetric transformation strain $\frac{\Delta V}{V}$, the driving force of Greenwood and Johnson (1965)'s mechanism;
- it is proportional to $\frac{\Sigma_{eq}^2}{E \bar{\sigma}_M}$, being thus an increasing function of Σ (as naturally expected), and a decreasing function of both E and $\bar{\sigma}_M$ (there is no elasticity-dependent transformation plasticity if the daughter-phase is elastically very stiff, or the mother-phase plastically very hard);
- collinearity with Σ' ensures incompressibility;
- the factors $[1 + k_3 e_1 (1 - e_1)]$ and $(1 - f)^4$ were required for a good fit with the numerical results;
- again, the parameters k_2 and k_3 are dimensionless and thus may be expected to be material-independent.

4.4 Final comparison between numerical results and theoretical predictions

The transformation plastic strain rate $\dot{\mathbf{E}}^{tp}$ being finally taken in the form

$$\dot{\mathbf{E}}^{tp} = \dot{\mathbf{E}}^{tp\ theor} + \dot{\mathbf{E}}^{corr1} + \dot{\mathbf{E}}^{corr2} \quad (58)$$

with $\dot{\mathbf{E}}^{tp\ theor}$, $\dot{\mathbf{E}}^{corr1}$ and $\dot{\mathbf{E}}^{corr2}$ given by equations (55), (56) and (57) respectively, Figure 11 illustrates the comparison between model values and numerical results for the axial

transformation plastic strain E_3^{tp} as a function of the fraction f of daughter-phase, obtained under various tensile and compressive axial stresses, for various RVE eccentricities e_1 . The agreement is very good in all cases.

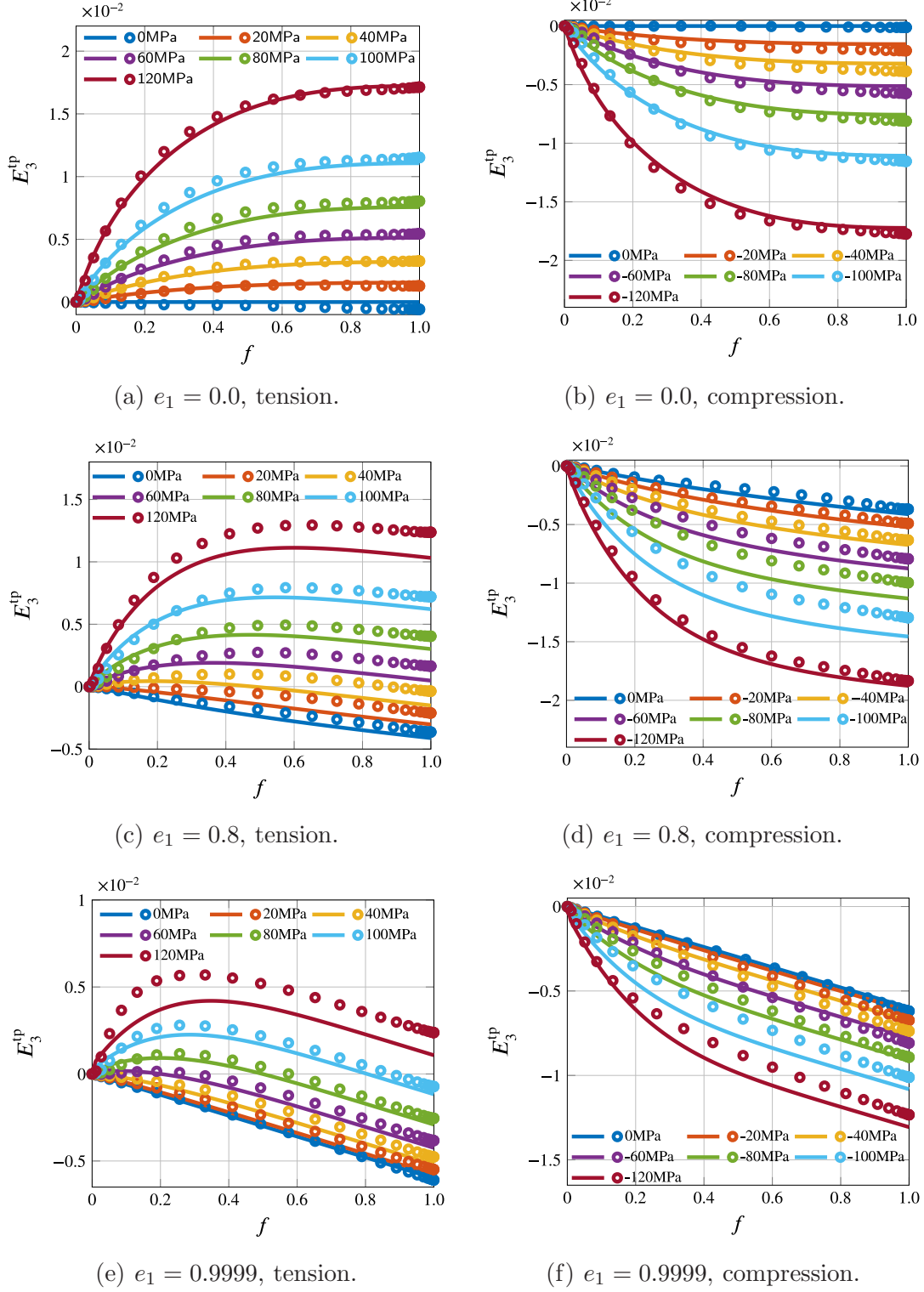


Fig. 11. Comparison of theoretical and numerical values of the axial transformation plastic strain versus volume fraction of daughter-phase, under various tensile and compressive axial stresses applied, for various RVE eccentricities e_1 .

It is also naturally interesting to consider multiaxial loads. Figure 12 again illustrates the comparison between model predictions and numerical results for the axial transformation plastic strain E_3^{tp} , but now under combination of a tensile stress Σ_3 and a shear stress Σ_{23} . The numbers in the figures provide the values of Σ_3 , and the ratio Σ_3/Σ_{23} amounts to 1 in the three figures on the left, and 2 in the three figures on the right. Again, the agreement between the model and the FFT-based simulations is very good.

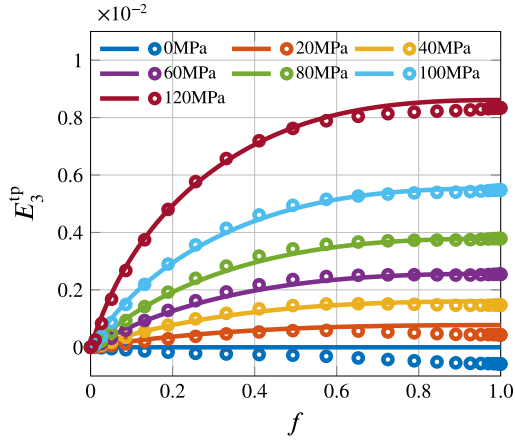
5 Synthesis and perspectives

This paper was devoted to an extension of El Majaty *et al.* (2018)'s recent modeling of Greenwood and Johnson (1965)'s mechanism of transformation plasticity of metals and alloys, initially limited to growing nuclei of daughter-phase of *spherical* shape, to nuclei of *prolate spheroidal* shape. The goal was essentially to incorporate into the model the possible influence upon transformation plasticity of *morphological anisotropies*, arising notably from growth of nuclei of elongated shape in laminated plates (Desalos, 1981). Like in El Majaty *et al.* (2018)'s previous work, the treatment was based on disregard of Magee (1966)'s mechanism, neglect of elasticity and use of the powerful theory of limit-analysis (*the theory for rigid-plastic materials*).

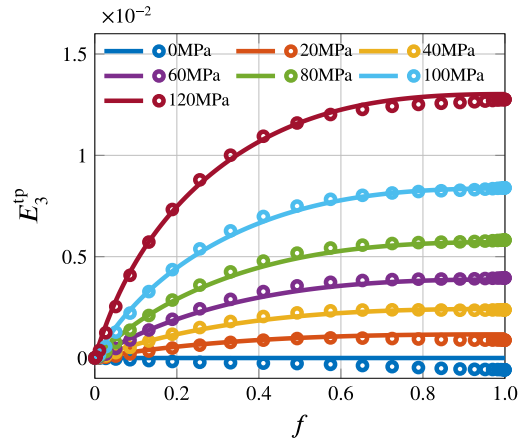
In Section 2, using the same analogy between problems of ductile rupture and transformation plasticity as in (El Majaty *et al.*, 2018), we began by extending Monchiet *et al.* (2014)'s limit-analysis-based study of a hollow prolate spheroidal RVE containing a stress-free confocal prolate spheroidal void, by including the possibility of some internal load applied on the void's boundary.

In Section 3, we showed how to apply the results obtained previously to transformation plasticity, by interpreting the sound domain of the RVE of Section 2 as representing the mother-phase gradually shrinking as a result of the transformation, and the internal loading as due to the correspondingly growing nucleus of daughter-phase, which expands as a result of the volumetric transformation strain (the relative difference of specific volume between the phases). The major result evidenced in this Section was the nonzero value of the transformation plastic strain even in the absence of application of any external load, due to the macroscopic anisotropy arising from the preferred orientation of the elongated nuclei of daughter-phase.

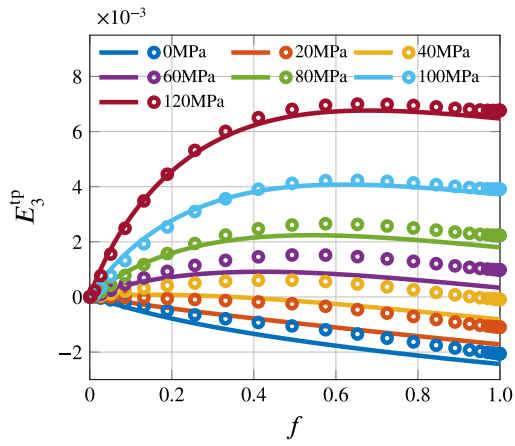
Finally in Section 4, we presented some simulations of Greenwood and Johnson (1965)'s mechanism of transformation plasticity in large RVEs containing many nuclei of growing daughter-phase, aimed at assessing and completing the theory developed, using an FFT-based numerical homogenization method (Moulinec and Suquet, 1998). These simulations, for spheroidal nuclei, paralleled those presented in a previous work for spherical ones (El Majaty *et al.*, 2021), similarly aimed at assessing (El Majaty *et al.*, 2018)'s model for such nuclei; but they evidenced an unexpected influence of the elasticity of the daughter-phase upon Greenwood and Johnson (1965)'s mechanism, negligible for spherical nuclei but of importance growing with their elongation. This influence was accounted for by introducing heuristic elastic corrections into the theoretical, limit-analysis-based expression of the



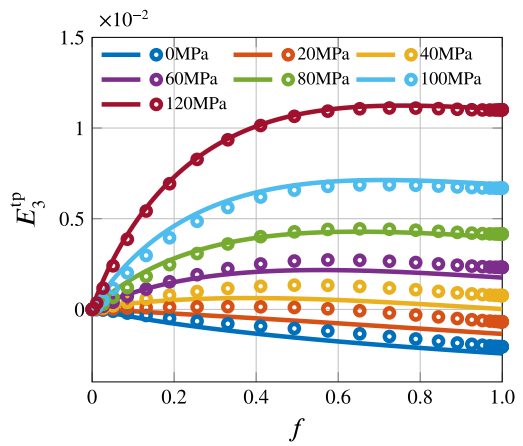
(a) $e_1 = 0.0$, $\Sigma_3/\Sigma_{23} = 1$.



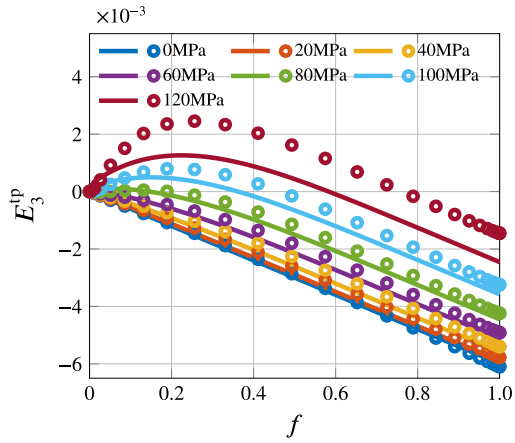
(b) $e_1 = 0.0$, $\Sigma_3/\Sigma_{23} = 2$.



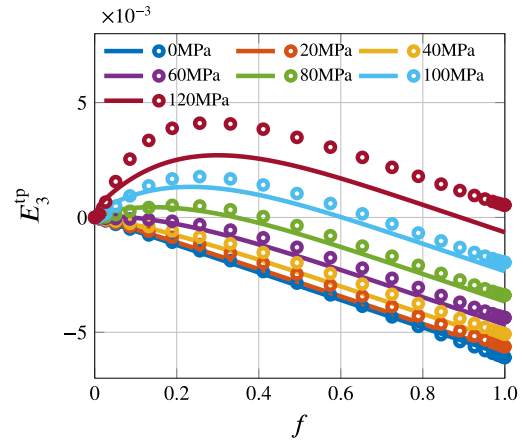
(c) $e_1 = 0.8$, $\Sigma_3/\Sigma_{23} = 1$.



(d) $e_1 = 0.8$, $\Sigma_3/\Sigma_{23} = 2$.



(e) $e_1 = 0.9999$, $\Sigma_3/\Sigma_{23} = 1$.



(f) $e_1 = 0.9999$, $\Sigma_3/\Sigma_{23} = 2$.

Fig. 12. Comparison of theoretical and numerical values of the axial transformation plastic strain versus volume fraction of daughter-phase, under various multiaxial loads, for various RVE eccentricities e_1 .

transformation plastic strain rate.

Perspectives include notably:

- Experimental studies of transformation plasticity coupled with observations of morphological anisotropies (metallurgical structure) after complete transformation. Although the impact of such anisotropies upon transformation plasticity has been known experimentally for quite some time, experiments do not seem to have been accompanied by such observations, compulsory to assess models of the kind developed here.
- Development of models aimed at predicting the elongation of growing nuclei of daughter-phase (a free, adjustable parameter in the present work!) as a function of the past mechanical history of the metallic component considered.
- Incorporation into the model of strain hardening effects in the mother-phase (disregarded in the present work based on the assumption of ideal plasticity, admittedly rather unrealistic at the temperatures of interest). Such a development could use a trick already employed by Gurson (1977) for this purpose in his pioneering work on plastic porous materials.
- Finally incorporation of the models developed in FE codes, permitting to better account for transformation plasticity during thermomechanical treatments, and thus leading to more accurate predictions of residual stresses and distortions.

References

- Barbe F., Quey R., Taleb L. (2007). Numerical modelling of the plasticity induced during diffusive transformation. Case of a cubic array of nuclei. *Eur. J. Mech. A/Solids*, **26**, 611-625.
- Barbe F., Quey R., Taleb L., Souza de Cursi E. (2008). Numerical modelling of the plasticity induced during diffusive transformation. An ensemble averaging approach for the case of random arrays of nuclei. *Eur. J. Mech. A/Solids*, **27**, 1121-1139.
- Barbe F., Quey R. (2011). A numerical modelling of 3D polycrystal-to-polycrystal diffusive phase transformations involving crystal plasticity. *Int. J. Plasticity*, **27**, 823-840.
- Cherkaoui M., Berveiller M., Lemoine X. (2000). Couplings between plasticity and martensitic phase transformation : overall behavior of polycrystalline TRIP steels. *Int. J. Plasticity*, **16**, 1215-1241.
- Coret M., Calloch S., Combescure A. (2002). Experimental study of the phase transformation plasticity of 16MND5 low carbon steel under multiaxial loading. *Int. J. Plasticity*, **18**, 1707-1727.
- Coret M., Calloch S., Combescure A. (2004). Experimental study of the phase transformation plasticity of 16MND5 low carbon steel induced by proportional and nonproportional biaxial loading paths. *Eur. J. Mech. A/Solids*, **23**, 823-842.
- Desalos Y. (1981). Comportement dilatométrique et mécanique de l'austénite métastable d'un acier A533. IRSID Report 95349401.
- Diani J.M., Sabar H., Berveiller M. (1995). Micromechanical modelling of the transformation induced plasticity (TRIP) phenomenon in steels. *Int. J. Engng. Sci.*, **33**, 1921-1934.
- Drucker D.C., Prager W. and Greenberg M.J. (1952). Extended limit-analysis theorems for continuous media, *Quart. Appl. Math.*, **9**, 381-389.
- El Majaty Y., Brenner R., Leblond J.B. (2021). FFT-based micromechanical simulations of transformation plasticity. Comparison with a limit-analysis-based theory. *Eur. J. Mech. A/Solids*, **86**, 104151.
- El Majaty Y., Leblond J.B., Kondo D. (2018). A novel treatment of Greenwood-Johnson's

- mechanism of transformation plasticity - Case of spherical growth of nuclei of daughter-phase. *J. Mech. Phys. Solids*, **121**, 175-197 (2018).
- Eshelby J. (1957). The determination of the elastic field of an ellipsoidal inclusion, and related problems. *Proc. Roy. Soc. London A*, **241**, 376-396.
- Fischlschweiger M., Cailletaud G., Antretter T. (2012). A mean field model for transformation induced plasticity including backstress effects for non-proportional loadings. *Int. J. Plasticity*, **37**, 53-71.
- Fukumoto M., Yoshizaki M., Imataka H., Okamura K. (2001). Three-dimensional FEM analysis of helical gear subjected to the carburized quenching process. *J. Soc. Mater. Sci. Japan*, **50**, 598-605.
- Ganghoffer J.F., Denis S., Gautier E., Simon A. (1993). Finite element calculation of the micromechanics of a diffusional transformation. *Eur. J. Mech. A/Solids*, **12**, 21-32.
- Greenwood G.W., Johnson R.H. (1965). The deformation of metals under small stresses during phase transformations. *Proc. Roy. Soc. London A*, **283**, 403-422.
- Gurson A.L. (1977). Continuum theory of ductile rupture by void nucleation and growth: Part I - Yield criteria and flow rules for porous ductile media. *ASME J. Engng. Mater. Technol.*, **99**, 2-15.
- Hill R. (1951). On the state of stress in a plastic-rigid body at the yield point, *Phil. Mag.*, **42**, 868-875.
- Hill R. (1967). The essential structure of constitutive laws of metal composites and polycrystals. *J. Mech. Phys. Solids*, **15**, 79-95.
- Leblond J.B., Devaux J., Devaux J.C. (1989). Mathematical modelling of transformation plasticity in steels – I: Case of ideal-plastic phases. *Int. J. Plasticity*, **5**, 551-572.
- Leblond J.B., Kondo D., Morin L., Remmal A. (2018). Classical and sequential limit-analysis revisited. *C.R. Mécanique*, **346**, 336-349.
- Leblond J.B., Mottet G., Devaux J.C. (1986a). A theoretical and numerical approach to the plastic behaviour of steels during phase transformations - I. Derivation of general relations. *J. Mech. Phys. Solids*, **34**, 395-409.
- Leblond J.B., Mottet G., Devaux J.C. (1986b). A theoretical and numerical approach to the plastic behaviour of steels during phase transformations - II. Study of classical plasticity for ideal-plastic phases. *J. Mech. Phys. Solids*, **34**, 411-432.
- Madou K., Leblond J.B. (2012). A Gurson-type criterion for porous ductile solids containing arbitrary ellipsoidal voids - I: Limit-analysis of some representative cell. *J. Mech. Phys. Solids*, **60**, 1020-1036.
- Magee C.L. (1966). *Transformation kinetics, microplasticity and ageing of martensite in Fe-31 Ni*. Ph.D. thesis, Carnegie-Mellon University, Pittsburgh.
- Mandel J. (1964). Contribution théorique à l'étude de l'écoulement plastique. In : *Proc. 11th Int. Congr. on Applied Mechanics*, Munich, pp. 502-509.
- Miyao K., Wang Z.G., Inoue T. (1986). Analysis of temperature, stress and metallic structure in carburized-quenched gear considering transformation plasticity. *J. Soc. Mater. Sci. Japan*, **35**, 1352-1357.
- Monchiet V., Charkaluk E., Kondo D. (2011). A micromechanics-based modification of the Gurson criterion by using Eshelby-like velocity fields. *Eur. J. Mech. A/Solids*, **30**, 940-949.
- Monchiet V., Charkaluk E., Kondo D. (2014). Macroscopic yield criteria for ductile materials containing spheroidal voids: An Eshelby-like velocity fields approach. *Mech. Mater.*,

72, 1-18.

- Moulinec H., Suquet P. (1998). A numerical method for computing the overall response of nonlinear composites with complex microstructures. *Comput. Meth. Appl. Mech. Engng.*, **157**, 69-94.
- Otsuka T., Brenner R., Bacroix B. (2018). FFT-based modelling of transformation plasticity in polycrystalline materials during diffusive phase transformation. *Int. J. Engng. Sci.*, **127**, 92-113.
- Taleb T., Petit S., Jullien J.F. (2004). Prediction of residual stresses in the heat-affected zone. *J. Physique IV*, **120**, 705-712.
- Taleb L., Sidoroff F. (2003). A micromechanical modeling of the Greenwood-Johnson mechanism in transformation induced plasticity. *Int. J. Plasticity*, **19**, 1821-1842.
- Vincent Y., Bergheau J.M., Leblond J.B. (2003). Viscoplastic behavior of steels during phase transformations. *C.R. Mécanique*, **331**, 587-594.
- Weisz-Paltrault (2017). Multiphase model for transformation induced plasticity. Extended Leblond's model. *J. Mech. Phys. Solids*, **106**, 152-175.

A Appendix : Monchiet *et al.* (2014)'s displacement fields for the prolate spheroidal geometry subjected to axisymmetric loadings

We refer here to Section 3 and Appendix A of Monchiet *et al.* (2014)'s paper. For a general, non-axisymmetric loading, the trial incompressible displacement fields¹³ considered by Monchiet *et al.* (2014) depend on 11 parameters: the 5 independent components of a traceless, symmetric second-rank tensor \mathbf{A} , and the 6 independent components of an arbitrary symmetric second-rank tensor \mathbf{D}^* .¹⁴ In the axisymmetric case, the sole possibly nonzero components of \mathbf{A} are $A_{11} = A_{22} \equiv A_1 = -A_{33}/2 \equiv -A_3/2$, and the sole possibly nonzero components of \mathbf{D}^* are $D_{11}^* = D_{22}^* \equiv D_1^*$ and $D_{33}^* \equiv D_3^*$; hence Monchiet *et al.* (2014)'s axisymmetric trial fields depend on 3 parameters only.

The detailed expressions of Monchiet *et al.* (2014)'s trial displacement fields are given by their equations (10) and (12), but will not be needed here. On the other hand the components of the corresponding overall external and internal strain tensors are given, in the axisymmetric case, by their equations (26):

$$\begin{cases} E_1 = -\frac{A_3}{2} + f \left[\frac{1}{2}(3 - 3\alpha_1 - \beta_1)D_1^* + \frac{\beta_1}{2}D_3^* \right] \\ E_3 = A_3 + f \left[(3\alpha_1 + \beta_1 - 1)D_1^* + (1 - \beta_1)D_3^* \right] \\ \bar{E}_1 = -\frac{A_3}{2} + \frac{1}{2}(3 - 3\alpha_f - \beta_f)D_1^* + \frac{\beta_f}{2}D_3^* \\ \bar{E}_3 = A_3 + (3\alpha_f + \beta_f - 1)D_1^* + (1 - \beta_f)D_3^*. \end{cases} \quad (\text{A.1})$$

We select, within the three-dimensional space of axisymmetric trial fields, a basis consisting of the three following fields:

- A field $\mathbf{u}^{(1)}$ having $A_1^{(1)} = A_3^{(1)} = 0$ and $D_1^{(1)*} = D_3^{(1)*} = \frac{1}{f}$.
- A field $\mathbf{u}^{(2)}$ having $A_1^{(2)} = -\frac{1}{2}$, $A_3^{(2)} = 1$ and $D_1^{(2)*} = D_3^{(2)*} = 0$.
- A field $\mathbf{u}^{(3)}$ having $A_1^{(3)} = A_3^{(3)} = 0$ and $D_1^{(3)*} = -\frac{1}{2f}$, $D_3^{(3)*} = \frac{1}{f}$.

Using equations (A.1), one then obtains equations (13), (14) and (15) of the text providing the individual components of the overall external and internal strain tensors corresponding to these three fields.

¹³ In fact Monchiet *et al.* (2014) did not define “displacement” but “velocity” fields; in the present context they are considered as “displacement” fields, from which “velocity” fields are obtained through time-differentiation (denoted with a dot).

¹⁴ In Monchiet *et al.* (2014)'s work the tensor \mathbf{D}^* was noted \mathbf{d}^* ; the notation \mathbf{D}^* is preferred here in order to avoid any possible confusion with the local strain rate tensor.

B Appendix : estimation of the overall plastic dissipation for Monchiet *et al.* (2014)'s axisymmetric velocity fields

B.1 A simplified formalism for axisymmetric second- and fourth-rank tensors

The first task in this Appendix is to define a formalism permitting to simplify linear algebraic operations on axisymmetric tensors.

- First, for any axisymmetric, symmetric second-rank tensor \mathbf{W} (with sole possibly nonzero components $W_{11} = W_{22}$ and W_{33}), we define a corresponding 2-dimensional vector \mathcal{W} of components

$$\begin{cases} \mathcal{W}_m = \lambda(2W_{11} + W_{33}) \\ \mathcal{W}_d = \mu(W_{33} - W_{11}) \end{cases} \quad (\text{B.1})$$

where λ and μ are parameters. The choice of these parameters is dictated by the requirement that it “preserve the scalar product” so that the relation

$$\mathbf{W} : \mathbf{W}' = W_{ij}W'_{ij} = \mathcal{W} \cdot \mathcal{W}' = \mathcal{W}_\alpha \mathcal{W}'_\alpha \quad (\text{B.2})$$

be satisfied for every \mathbf{W} and \mathbf{W}' ; a simple calculation then leads to the values

$$\lambda = \frac{1}{\sqrt{3}} \quad ; \quad \mu = \sqrt{\frac{2}{3}}. \quad (\text{B.3})$$

- Second, for any axisymmetric fourth-rank tensor \mathbb{L} possessing the minor symmetries $\mathbb{L}_{ijkl} = \mathbb{L}_{jikl} = \mathbb{L}_{ijlk}$, we define a corresponding 2-dimensional second-rank tensor (2×2 matrix) \mathcal{L} in such a way that for every axisymmetric, symmetric second-rank tensor \mathbf{W} ,

$$\mathbf{Z} = \mathbb{L} : \mathbf{W} \quad (Z_{ij} = \mathbb{L}_{ijkl}W_{kl}) \quad \Leftrightarrow \quad \mathcal{Z} = \mathcal{L} \cdot \mathcal{W} \quad (\mathcal{Z}_\alpha = \mathcal{L}_{\alpha\beta}W_\beta). \quad (\text{B.4})$$

Simple calculations based on equations (B.1) and (B.3) then provide the components of the tensor \mathcal{L} :

$$\begin{cases} \mathcal{L}_{mm} = \frac{1}{3}(2\mathcal{L}_{1111} + 2\mathcal{L}_{1122} + 2\mathcal{L}_{1133} + 2\mathcal{L}_{3311} + \mathcal{L}_{3333}) \\ \mathcal{L}_{md} = \frac{\sqrt{2}}{3}(-\mathcal{L}_{1111} - \mathcal{L}_{1122} + 2\mathcal{L}_{1133} - \mathcal{L}_{3311} + \mathcal{L}_{3333}) \\ \mathcal{L}_{dm} = \frac{\sqrt{2}}{3}(-\mathcal{L}_{1111} - \mathcal{L}_{1122} - \mathcal{L}_{1133} + 2\mathcal{L}_{3311} + \mathcal{L}_{3333}) \\ \mathcal{L}_{dd} = \frac{1}{3}(\mathcal{L}_{1111} + \mathcal{L}_{1122} - 2\mathcal{L}_{1133} - 2\mathcal{L}_{3311} + 2\mathcal{L}_{3333}). \end{cases} \quad (\text{B.5})$$

Note that if \mathbb{L} possesses the major symmetries $\mathbb{L}_{ijkl} = \mathbb{L}_{klij}$, \mathcal{L} is itself symmetric ($\mathcal{L}_{md} = \mathcal{L}_{dm}$).

- Finally it is easy to see that the second-rank tensor corresponding to the transpose of \mathbb{L} (of components $\mathbb{L}_{ijkl}^T = \mathbb{L}_{klij}$) is simply the transpose of \mathcal{L} (of components $\mathcal{L}_{\alpha\beta}^T = \mathcal{L}_{\beta\alpha}$).

One thus sees that with such a formalism, complex tensorial operations on axisymmetric fourth-rank tensors reduce to simple matrix operations on 2×2 matrices.

B.2 Calculation of some tensors

The first tensor playing an important role in Monchiet *et al.* (2014)'s work is Eshelby (1957)'s tensor $\mathbb{S}(e)$ for a prolate spheroidal inclusion of eccentricity e , embedded in an infinite elastic *incompressible* medium (Poisson's ratio $\nu = 1/2$). The components of this tensor are given by equations (20) of their paper. The components of the associated 2-dimensional second-rank tensor \mathcal{S} are easily deduced from equations (B.5):

$$\begin{cases} \mathcal{S}_{mm} = 1 \\ \mathcal{S}_{dm} = \frac{1}{\sqrt{2}}[3\alpha(e) - 1] \end{cases} ; \quad \begin{cases} \mathcal{S}_{md} = 0 \\ \mathcal{S}_{dd} = \frac{3}{2}[1 - \alpha(e) - \beta(e)]. \end{cases} \quad (\text{B.6})$$

A second important tensor is noted $\mathbb{L}(e)$ in Monchiet *et al.* (2014)'s work; its components are given by equations (C.6) of their paper, and those of the corresponding 2-dimensional second-rank tensor \mathcal{L} by

$$\begin{cases} \mathcal{L}_{mm} = 2 \\ \mathcal{L}_{dm} = \mathcal{L}_{md} = \frac{1}{\sqrt{2}}[1 - 3\alpha(e)] \\ \mathcal{L}_{dd} = \frac{1}{2}[-1 + 3\alpha(e) + 3\beta(e)]. \end{cases} \quad (\text{B.7})$$

Note that this tensor is symmetric.

Two additional tensors are defined from there: first, a tensor \mathbb{P} defined by (equation (C.5) of Monchiet *et al.* (2014):

$$\begin{aligned} \mathbb{P} &= \frac{1}{1-f} [\mathbb{S}^T(e_f) : \mathbb{L}(e_f) - f\mathbb{S}^T(e_1) : \mathbb{L}(e_1)] \\ \Leftrightarrow \mathcal{P} &= \frac{1}{1-f} [\mathcal{S}^T(e_f) : \mathcal{L}(e_f) - f\mathcal{S}^T(e_1) : \mathcal{L}(e_1)]; \end{aligned} \quad (\text{B.8})$$

the components of \mathcal{P} are easily deduced from equations (B.5):

$$\begin{cases} \mathcal{P}_{mm} = 2 + \frac{f(1 - 3\alpha_1)^2 - (1 - 3\alpha_f)^2}{2(1 - f)} \\ \mathcal{P}_{dm} = \mathcal{P}_{md} = \frac{3}{2\sqrt{2}(1 - f)} [(1 - 3\alpha_f)(1 - \alpha_f - \beta_f) - f(1 - 3\alpha_1)(1 - \alpha_1 - \beta_1)] \\ \mathcal{P}_{dd} = \frac{3}{4(1 - f)} [f(1 - \alpha_1 - \beta_1)(1 - 3\alpha_1 - 3\beta_1) - (1 - \alpha_f - \beta_f)(1 - 3\alpha_f - 3\beta_f)]; \end{cases} \quad (\text{B.9})$$

again, this tensor is symmetric. Also, Monchiet *et al.* (2014) define a last tensor \mathbb{Q} through their equation (C.2):

$$\mathbb{Q} = \frac{1}{1-f} [\mathbb{S}(e_1) - \mathbb{S}(e_f)] \quad \Leftrightarrow \quad \mathcal{Q} = \frac{1}{1-f} [\mathcal{S}(e_1) - \mathcal{S}(e_f)]; \quad (\text{B.10})$$

the components of \mathcal{Q} are given by

$$\begin{cases} \mathcal{Q}_{mm} = 0 \\ \mathcal{Q}_{dm} = \frac{3}{\sqrt{2}(1-f)}(\alpha_1 - \alpha_f) \end{cases} ; \quad \begin{cases} \mathcal{Q}_{md} = 0 \\ \mathcal{Q}_{dd} = \frac{1}{2(1-f)}(3\alpha_f + 2\beta_f - 3\alpha_1 - 2\beta_1). \end{cases} \quad (\text{B.11})$$

B.3 Monchiet *et al.* (2014)'s formula for the overall dissipation and its modifications

Monchiet *et al.* (2014)'s formula for the overall dissipation \mathcal{D} reads (see their equations (29) and (B.8):

$$\begin{aligned} \frac{\mathcal{D}}{\text{vol}(\Omega)} &\simeq \bar{\sigma}_M f \int_f^1 \left[A_{eq}^2 + \frac{2}{3} (\mathbf{D}^* : \mathbb{P} : \mathbf{D}^* + 2\mathbf{A} : \mathcal{Q} : \mathbf{D}^*) u^2 \right]^{1/2} \frac{du}{u^2} \\ &= \bar{\sigma}_M f \int_f^1 \left[A_{eq}^2 + \frac{2}{3} (\mathcal{D}^* \cdot \mathcal{P} \cdot \mathcal{D}^* + 2\mathcal{A} \cdot \mathcal{Q} \cdot \mathcal{D}^*) u^2 \right]^{1/2} \frac{du}{u^2}. \end{aligned} \quad (\text{B.12})$$

In this equation:

- One integrates over successive spheroids confocal with the surface of the void and the external boundary, each spheroid being characterized by the parameter $u = \frac{a_f b_f^2}{ab^2}$ with a and b denoting its major and minor semi-axes.
- The tensors \mathbf{A} and \mathbf{D}^* are those corresponding, in the sense of Appendix A, to the general trial velocity field $\dot{\mathbf{u}}(\mathbf{x})$ resulting from time-differentiation of the general displacement field $\mathbf{u}(\mathbf{x})$ defined by (16); it follows from the values of these tensors for the displacement fields $\mathbf{u}^{(1)}$, $\mathbf{u}^{(2)}$, $\mathbf{u}^{(3)}$, given in Appendix A, that

$$\begin{cases} A_1 = -\frac{\dot{q}_2}{2} \\ A_3 = \dot{q}_2 \end{cases} ; \quad \begin{cases} D_1^* = \frac{\dot{q}_1}{f} - \frac{\dot{q}_3}{2f} \\ D_3^* = \frac{\dot{q}_1}{f} + \frac{\dot{q}_3}{f} \end{cases} \quad (\text{B.13})$$

- $A_{eq} \equiv (\frac{2}{3}\mathbf{A} : \mathbf{A})^{1/2}$ denotes the von Mises norm of the traceless tensor \mathbf{A} in the sense of strain rates.

We now introduce two approximations not made by Monchiet *et al.* (2014), but which are perfectly admissible in the case of *prolate* spheroids and lead to a greatly simplified final expression of the overall dissipation. Both of these approximations are based on consideration of the two extreme cases where the prolate (internal and external) spheroids become either *spherical* or *cylindrical* (infinitely elongated); by equations (3) and (5), the first case corresponds to $e_f = e_1 = 0$, $\alpha_f = \alpha_1 = \frac{1}{3}$, $\beta_f = \beta_1 = \frac{2}{5}$, and the second to $e_f = e_1 = 1$, $\alpha_f = \alpha_1 = 0$, $\beta_f = \beta_1 = 1$.

First, it was remarked by Monchiet *et al.* (2014) themselves, and it is easily checked using the expressions (B.11) of the components of the tensor \mathcal{Q} , that the ‘‘crossed’’ term $2\mathcal{A} \cdot \mathcal{Q} \cdot \mathcal{D}^*$ in the expression (B.12)₂ of the overall dissipation is nil in the two extreme, spherical and cylindrical cases. It thus seems reasonable to neglect this crossed term in all

intermediary cases where the eccentricities e_f and e_1 are neither zero nor unity. Equation (B.12) then becomes

$$\begin{aligned}\frac{\mathcal{D}}{\text{vol}(\Omega)} &\simeq \bar{\sigma}_M f \int_f^1 \left(A_{eq}^2 + \frac{2}{3} \mathcal{D}^* \cdot \mathcal{P} \cdot \mathcal{D}^* u^2 \right)^{1/2} \frac{du}{u^2} \\ &= \bar{\sigma}_M f \int_f^1 \left[A_{eq}^2 + \frac{2}{3} \left(\mathcal{P}_{mm} \mathcal{D}_m^{*2} + \mathcal{P}_{dd} \mathcal{D}_d^{*2} + 2\mathcal{P}_{md} \mathcal{D}_m^* \mathcal{D}_d^* \right) u^2 \right]^{1/2} \frac{du}{u^2}.\end{aligned}\quad (\text{B.14})$$

Second, it may also be remarked that according to the expressions (B.9) of the components of the tensor \mathcal{P} , the other ‘‘crossed’’ term $2\mathcal{P}_{md} \mathcal{D}_m^* \mathcal{D}_d^*$ in the expression (B.14) of the overall dissipation is also nil in the two extreme spherical and cylindrical cases, so that it also seems reasonable to neglect it in all intermediary cases. Equation (B.14)₂ then becomes

$$\frac{\mathcal{D}}{\text{vol}(\Omega)} \simeq \bar{\sigma}_M f \int_f^1 \left[A_{eq}^2 + \frac{2}{3} \left(\mathcal{P}_{mm} \mathcal{D}_m^{*2} + \mathcal{P}_{dd} \mathcal{D}_d^{*2} \right) u^2 \right]^{1/2} \frac{du}{u^2}.\quad (\text{B.15})$$

Now by equations (B.1), (B.3) and (B.13), $A_{eq}^2 = \dot{q}_2^2$, $\mathcal{D}_m^* = \sqrt{3} \frac{\dot{q}_1}{f}$ and $\mathcal{D}_d^* = \sqrt{\frac{3}{2}} \frac{\dot{q}_3}{f}$, so that equation (B.15) takes the form

$$\frac{\mathcal{D}}{\text{vol}(\Omega)} \simeq \bar{\sigma}_M \int_f^1 \left[f^2 \dot{q}_2^2 + \left(2\mathcal{P}_{mm} \dot{q}_1^2 + \mathcal{P}_{dd} \dot{q}_3^2 \right) u^2 \right]^{1/2} \frac{du}{u^2}.\quad (\text{B.16})$$

Unfortunately equation (B.16) raises the following issue. In the spherical case where $\alpha_f = \alpha_1 = \frac{1}{3}$ and $\beta_f = \beta_1 = \frac{2}{5}$, this equation becomes, by equation (B.9):

$$\frac{\mathcal{D}}{\text{vol}(\Omega)} \simeq \bar{\sigma}_M \int_f^1 \left[f^2 \dot{q}_2^2 + \left(4\dot{q}_1^2 + \frac{6}{25} \dot{q}_3^2 \right) u^2 \right]^{1/2} \frac{du}{u^2}.\quad (\text{B.17})$$

But prior to Monchiet *et al.* (2014)’s limit-analysis of a hollow *spheroid*, these authors performed a similar analysis of a hollow *sphere*, with a slightly different result (Monchiet *et al.*, 2011):

$$\frac{\mathcal{D}}{\text{vol}(\Omega)} \simeq \bar{\sigma}_M \int_f^1 \left[f^2 \dot{q}_2^2 + \left(4\dot{q}_1^2 + \frac{6}{25} g(f) \dot{q}_3^2 \right) u^2 \right]^{1/2} \frac{du}{u^2} \text{ with } g(f) = 1 - 4f \frac{(1 - f^{2/3})^2}{1 - f}.\quad (\text{B.18})$$

Equations (B.17) and (B.18) are equivalent only in the case of small porosities ($f \ll 1$, $g(f) \simeq 1$). The hypothesis of small porosity was made in (Monchiet *et al.*, 2014) (implicitly in their Appendix C) but not in (Monchiet *et al.*, 2011), which explains the difference between expressions (B.17) and (B.18).

In the context of ductile rupture considered in the works of Monchiet *et al.* (2011) and Monchiet *et al.* (2014), the hypothesis of small porosity is perfectly acceptable. (The porosity *may* take larger values, but then new phenomena such as coalescence of cavities set in, thus anyway invalidating models of void growth of the type developed in (Monchiet *et al.*, 2011) and (Monchiet *et al.*, 2014)). But in the context of transformation plasticity envisaged in this paper, the situation is different. The parameter f no longer represents the volume fraction of voids but that of the daughter-phase, which spans the entire interval

$[0, 1]$ when the transformation from the mother- to the daughter-phase proceeds. The hypothesis $f \ll 1$ is thus no longer acceptable.

It thus becomes indispensable to repeat the treatment of Monchiet *et al.* (2014) by dropping the hypothesis $f \ll 1$. Without entering into details, it will suffice to say that such an improved treatment leads to the same expression (B.16) of the overall dissipation - identical to equation (20) of the text - but for an expression of the component \mathcal{P}_{dd} of the tensor \mathcal{P} slightly corrected through introduction of some multiplicative factor $g(f, e_1)$, given by equation (22) of the text.

C Appendix : Numerical method for solving the system of coupled nonlinear equations on S and S_H

It is easy to check that the equations on S and S_H obtained, as indicated in Subsection 3.5, from combination of equation (54), the criterion (29) and the expression of S_H^2 resulting from (28)₃, are complex in S_H but *quadratic* in S ; that is, the system is of the form

$$\begin{cases} A_1(S_H)S^2 + B_1(S_H)S + C_1(S_H) = 0 \\ A_2(S_H)S^2 + B_2(S_H)S + C_2(S_H) = 0 \end{cases} \quad (\text{C.1})$$

with complex expressions of the coefficients $A_1(S_H)$, $B_1(S_H)$, $C_1(S_H)$, $A_2(S_H)$, $B_2(S_H)$, $C_2(S_H)$. This permits to eliminate the term in S^2 between these equations so as to obtain an algebraic equation of the first degree on S , the solution of which is

$$S = -\frac{A_1(S_H)C_2(S_H) - A_2(S_H)C_1(S_H)}{A_1(S_H)B_2(S_H) - A_2(S_H)B_1(S_H)}. \quad (\text{C.2})$$

Reinserting this result into either of equations (C.1), one gets a nonlinear equation on the sole variable S_H , which may be solved numerically by various methods, most simply a dichotomy.¹⁵

¹⁵ Again, such a method is facilitated by the *a priori* knowledge of the possible interval of variation of the variable S_H , $|S_H| \leq \bar{\sigma}_M \ln \frac{1}{f}$.